SEMMELWEIS EGYETEM

DOKTORI ISKOLA

# Ph.D. értekezések

# 3281.


## Nagy Attila Gergő


**Funkcionális Idegtudományok**

című program

Programvezető: Dr. Sperlágh Beáta, egyetemi tanár

Témavezető: Dr. Hájos Norbert, laborvezető

# ANATOMICAL INVESTIGATIONS OF THE SOURCE OF PERISOMATIC EXCITATORY INPUTS ON PARVALBUMIN-EXPRESSING INTERNEURONS IN THE DENTATE GYRUS AND THE DISTRIBUTION OF TRPC6 CHANNELS IN THE HIPPOCAMPUS

**PhD thesis**

**Attila Gergő Nagy**

János Szentágothai Neurosciences Doctoral School

Semmelweis University


Supervisor: Norbert Hájos, DSc

Official reviewers: Hajnalka Ábrahám, PhD

Gergely Zachar, PhD

Head of the Complex Examination Committee: Alán Alpár, DSc

Members of the Complex Examination Committee: Zsolt Borhegyi, PhD

Árpád Dobolyi, DSc

Budapest

2026

Table of Contents

Abbreviations

*AAC – axo-axonic cell*

*AIS – axon initial segment*

*AP – action potential*

*BC – basket cell*

*BiStr – bistratified*

*CA - cornu ammonis*

*CB – calbindin*

*CCK – cholecystokinin*

*CIRC - calcium-induced calcium release*

*CR – calretinin*

*CRH – corticotropin-releasing hormone*

*DAB – diaminobenzidine*

*DAB-Ni – Nickel-intensified diaminobenzidine*

*DG - dentate gyrus*

*EC – entorhinal cortex*

*EPSC – excitatory postsynaptic current*

*GABA – gamma-aminobutyric acid*

*GC - granule cell*

*GCL – granule cell layer*

*gl – str. granulosum*

*h - hilus*

*HICAP - hilar commissural-associational pathway related*

*HIL - hilar*

*HIPP - hilar perforant path -associated*

*iML – inner molecular layer*

*IN - interneuron*

*IPSC – inhibitory postsynaptic current*

*IS-IN – interneuron-specific interneuron*

*KO - knockout*

*LA – lacunosum-associated*

*LEC – lateral entorhinal cortex*

*luc – str. lucidum*

*MC – mossy cell*

*MEC – medial entorhinal cortex*

*mGluR – metabotropic glutamate receptor*

*ml – str. moleculare*

*mML – medial molecular layer*

*MOPP - molecular layer perforant path-associated*

*NGFC – neurogliaform cell*

*nNOS – neuronal nitric oxide synthase*

*NPY – neuropeptide Y*

*O-LM – oriens – lacunosum-moleculare*

*OML – outer molecular layer*

*oML – outer molecular layer cell*

*or – str. oriens*

*PaS – parasubiculum*

*PC - principal cell*

*PLC – phospholipase-C*

*PPA – perforant path-associated*

*PrS – presubiculum*

*PSD – postsynaptic density*

*PV – parvalbumin*

*PV-IR – parvalbumin-immunoreactive neuron*

*PYR - pyramidal cell*

*pyr – str. pyramidale*

*rad – str. radiatum*

*RADI – radiatum-associated*

*ret. spl. – retrosplenial cortex*

*RyR2 – ryanodine receptor type 2*

*SCA – Schaffer collateral-associated*

*sept. – septum*

*SGC – semilunar granule cell*

*SGC-PV – parvalbumin-immunoreactive interneuron contacting semilunar granule cell*

*slm – str. lacunosum-moleculare*

*SOM – somatostatin*

*SO-SO – stratum oriens – stratum oriens*

*str. - stratum*

*TML – total molecular layer cell*

*vGlut3 – vesicular glutamate transporter type 3*

*VIP – vasoactive intestinal polypeptide*

*WT – wild type*

# 1. INTRODUCTION

The hippocampal formation plays a fundamental role in several cognitive processes such as episodic memory formation or spatial navigation. It is an anatomical and functional unit formed by the entorhinal cortex, subiculum, parasubiculum, presubiculum and the hippocampus. The hippocampus itself is a 3-layered, allocortical structure that is built up by the hippocampus proper (or *Cornu Ammonis*) and the dentate gyrus (DG). These three layers are either densely packed with the somata of the principal neurons that reside here or mainly consist of axonal and dendritic processes and passing fibers arriving from other brain regions [1–5].

## 1.1 General anatomy of the rodent hippocampus

Similarly to other cortical regions, most of the neurons in the hippocampus are categorized as either principal cells (PCs) or interneurons (INs), two groups that are functionally and morphologically distinct. In terms of their abundance and connectivity patterns, PCs make up the majority of the local neurons and also give rise to projections that target different brain regions [5]. In contrast to PCs, INs arborize locally and are less abundant than PCs but they are extremely diverse, especially in the hippocampus [5,6].

PCs in the DG are called granule cells (GCs). In contrast, PCs in the hippocampus proper are the pyramidal cells (PYR). Both PC groups are glutamatergic, excitatory cells and their somata reside in a separate layer within the DG and the hippocampus proper (*stratum (str.) granulosum* and *str. pyramidale*, respectively) [7].

In the DG, the *str. granulosum* or granule cell layer contains the somata of the GCs [7]. The molecular layer (*str. moleculare*) contains the apical dendrites of the GCs. Finally, the hilus (or polymorphic layer) forms the 3$^{rd}$ layer which hosts the GC axons, somata of different types of INs and the mossy cells (MC).

The hippocampus proper is further subdivided into the *Cornu Ammonis* (CA) 1, CA2 and CA3 subregions. The somata of the PYR are located in the *str. pyramidale* (pyramidal layer). The PYR proximal apical dendrites occupy the *str. radiatum*, while the distal

apical dendrites the *str. lacunosum-moleculare*. The basal dendrites reside in the *str. oriens* **(Fig. 1)** [7,8].

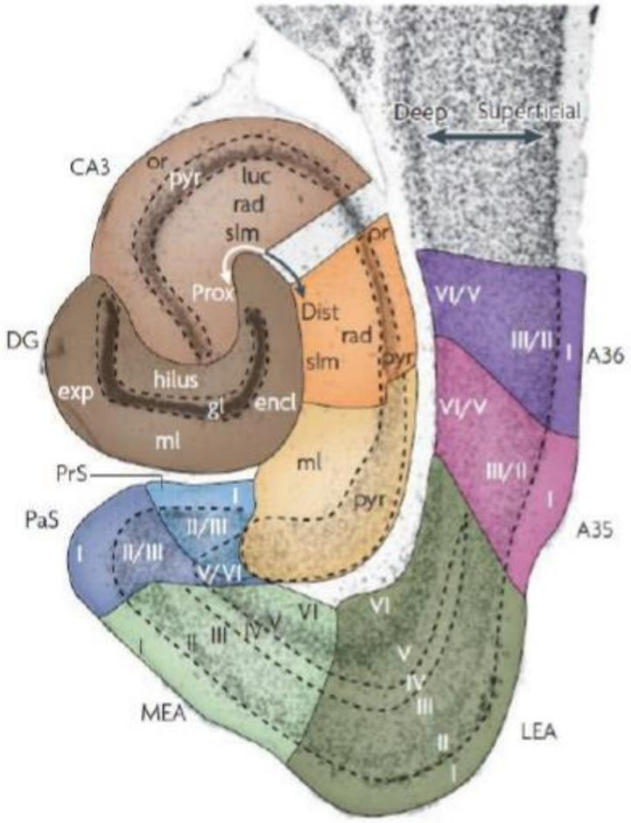


**Figure 1. Pseudocolored Nissl-stained horizontal section of the rat hippocampal formation.** *The different colors indicate distinct units of the hippocampal formation. Dark brown: DG, Light brown: CA3 subregion of hippocampus proper, Orange: CA1 subregion of the hippocampus proper, Yellow: Subiculum, Blue: Para- and presubiculum, Green: Later and medial entorhinal cortices. Abbreviations: DG – DG, CA – cornu ammonis, ml – str. moleculare, gl – str. granulosum, or – str. oriens, luc – str. lucidum, rad – str. radiatum, slm – str. lacunosum-moleculare, pyr – str. pyramidale, PrS – presubiculum, PaS – parasubiculum, MEA – medial entorhinal cortex, LEA – lateral entorhinal cortex. Note that the CA2 is not labeled here. Source:* [8] , *modified.*

1.2 The trisynaptic loop

The hippocampal formation forms extensive long-range connections with cortical regions and the DG is a main entry point of multimodal cortical information [9]. The dentate GCs are part of the trisynaptic loop; a significant route of information flow through the hippocampus [10]. A key importance of this route in hippocampal information processing arises from the fundamental role of the DG networks in pattern separation. In essence, pattern separation is a process during which the DG circuits map the overlapping, multimodal cortical representations to sparsely coded, orthogonal, non-overlapping representations [11–13].

To introduce how the DG is integrated into hippocampal information flow, next I will briefly overview the elements of the trisynaptic loop.

As the first step of the trisynaptic loop, the DG receives multimodal cortical information via the perforant path from the entorhinal cortex (EC) (10). Layer II (LII) EC neurons give rise to the part of the perforant path that forms synapses on the spines of distal dendrites of the GCs in the DG [14]. This is the '1$^{st}$ synapse' of the trisynaptic loop. The connection from the EC to the DG is unidirectional and, similarly to other projections in the hippocampus, shows a topographical order: the axons from the lateral EC form synapses in the outer 1/3 of the molecular layer, while axons from the medial EC terminate in the middle third. In rodents approximately 50,000 EC neurons diverge to 500,000 GCs [13,15,16]. This anatomical motif is fundamental to pattern separation.

The '2$^{nd}$ synapse' of the trisynaptic loop is established by the axons of DG GCs that form the mossy fibers and terminate on CA3 PYRs in the str. lucidum (named after the optical characteristics lent to this stratum by the mossy fibers). These axons enter the hilus and, while forming synapses on hilar neurons, project to the CA3 and form synapses on both PYRs and INs [17–20]. In contrast to the divergence seen in case of the perforant path, here, at the DG to CA3 projection, the axons of GCs terminate only on a few (10-15) CA3 PYR, keeping the conveyed information still separately. CA3 PYR, however, are interconnected with each other via their recurrent collaterals, allowing the CA3 circuits to perform pattern completion [21].

The last element of the trisynaptic loop is formed by the axons of CA3 PYR that form the Schaffer collaterals and innervate the proximal apical dendrites of CA1 PYRs in the str.

radiatum and their basal dendrites in the str. oriens. Finally, the CA1 PYRs project out from the hippocampus and send their axons to their subicular postsynaptic partners.

### 1.3 Examples of the complexity of hippocampal connectivity

It is beyond the scope of this dissertation, but here I would like to note that the hippocampal connections are far more complex and elaborate than the trisynaptic circuit. For example, the EC projects to the hippocampus through a number of other pathways as well. One such projection is the temporo-ammonic pathway (TA) (or the indirect route) that is mainly, but not exclusively, formed by the EC Layer III (LIII) PC axons that innervate the CA1. In contrast to the Schaffer collaterals, the TA pathway forms its synapses on the CA1 PYR distal dendrites in the *str. lacunosum-moleculare*. The MEC projects to the proximal CA1 PCs (i.e., closer to the CA3), while the LEC provides inputs on the dendrites of distal CA1 PCs (i.e., closer to the subiculum). This pathway has been suggested to play an important role for example, in spatial navigation [22,23], memory consolidation [24] or in modulating the plasticity of Schaffer collateral synapses [22,25–27]. Finally, PCs in the LEC and MEC are innervated by PYRs that they target in the CA1, thus, these two pathways form independent loops that could process information from the LEC and MEC separately [22].

Apart from the cortical projections, the hippocampus also forms a wealth of intrinsic, commissural and subcortical connections as well. For example, the commissural-associational fibers in the DG are made up mostly by MC axons and to a lesser extent by the axons of GABAergic neurons. The MC axonal collaterals form synapses in the contralateral DG on the proximal dendrites of GCs and INs [28]. Moreover, the hippocampus is also heavily interconnected with subcortical structures such as the medial septum. This projection has been shown to be heavily involved in generating hippocampal theta rhythmic activity, a fundamental scaffold of hippocampal communications [29,30].

### 1.4 Interneurons of the hippocampus

GABAergic INs show great anatomical and physiological heterogeneity and play a fundamental role in the precise spatiotemporal regulation of the neuronal activity [31].

Functionally relevant IN populations have been defined using a combination of morphological, physiological, developmental properties and neurochemical markers [6,32,33]. Using these criteria, 29 different types of INs have been identified in the hippocampus proper alone [32], some of which are also present in the neocortex (**Fig. 2**).

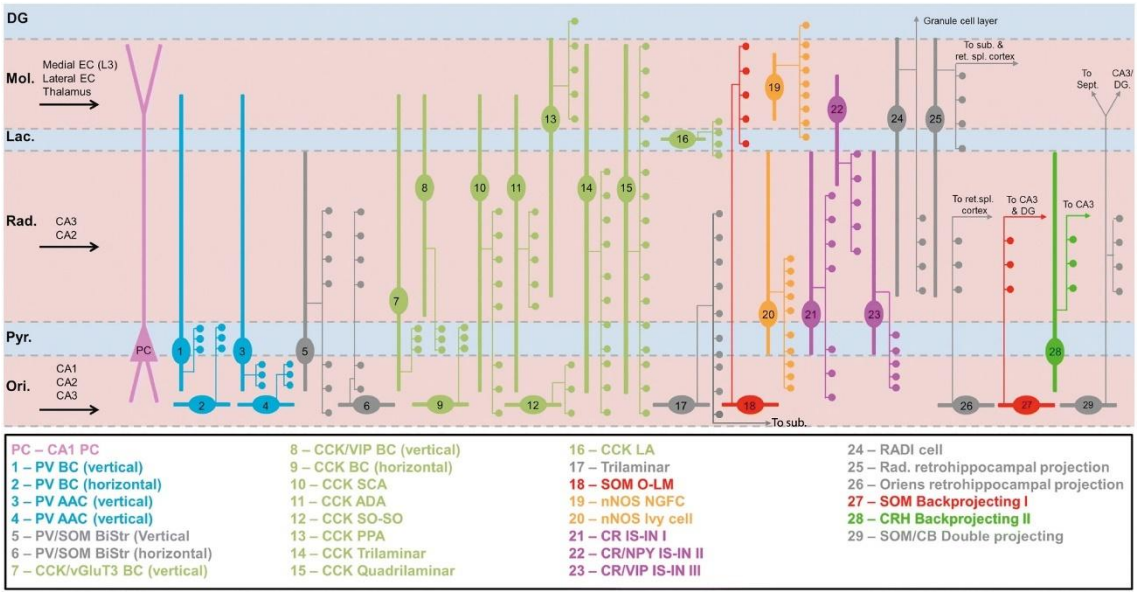


**Figure 2. Schematic representation of the different IN types in the hippocampus proper.** *A summary of the IN types in the hippocampus proper, defined by their neurochemical markers and morphological patterns. Thick lines represent the dendrites and axons. Small circles represent the major areas where the terminals are formed. Colors represent neurochemically defined groups. Abbreviations: PV – parvalbumin, BC – basket cell, AAC – axo-axonic cell, SOM – somatostatin, BiStr – bistratified cell, CCK – cholecystokinin, vGluT3 – vesicular glutamate transporter type 3, VIP – vasoactive intestinal polypeptide, SCA – Schaffer collateral-associated interneuron, SO-SO – stratum oriens – stratum oriens interneuron, PPA – perforant path-associated interneuron, LA – lacunosum-associated interneuron, O-LM – oriens – lacunosum-moleculare cell, NGFC – neurogliaform cell, nNOS – neuronal nitric oxide synthase, CR – calretinin, IS-IN – interneuron-specific interneuron, NPY – neuropeptide Y, RADI – radiatum-associated interneuron, CRH – corticotropin-releasing hormone, CB – calbindin, ret. spl. – retrosplenial cortex, sept. - septum. Source:* [32]

Based on which subcellular domain they innervate; two large populations of the INs are the perisomatic region-targeting INs and the dendrite-targeting INs. The perisomatic region-targeting INs target the perisomatic region of the PCs (proximal dendrites, somata, axon initial segments), while the dendrite-targeting INs form their synapses on the distal dendrites of the PCs [6,34]. The former INs can control the output (i.e., the spiking) of their targets, whereas the latter can regulate the impacts of incoming information.

For the perisomatic region-targeting IN population for example parvalbumin (PV) has proven to be a relevant neurochemical marker [6,35], meanwhile, for the dendrite-targeting INs somatostatin (SOM) is widely used [32,36] for labeling. Other markers also identify distinct groups of INs: for example mGluR1a receptor subunit is also expressed by a large population of hippocampal INs [36].

The mGluR1a-expressing cells are typical feedback inhibitory cells, since most of their excitatory input originates from those PCs that they innervate [37]. On the other hand, feed-forward inhibition [38,39] in the hippocampal formation is predominantly accomplished by PV-immunoreactive INs (PV-IRs), whose spiking is very effectively driven by excitatory afferents in a feed-forward manner [40]. Thus, distinct inhibitory cell types are specialized to control the different computational domains of PCs in the hippocampal formation [33] .

A detailed summary of the hippocampal INs is far beyond the constraints of this dissertation. Therefore, in the next sections, I aim to overview examples of IN types that I deemed most important for interpreting the presented results.

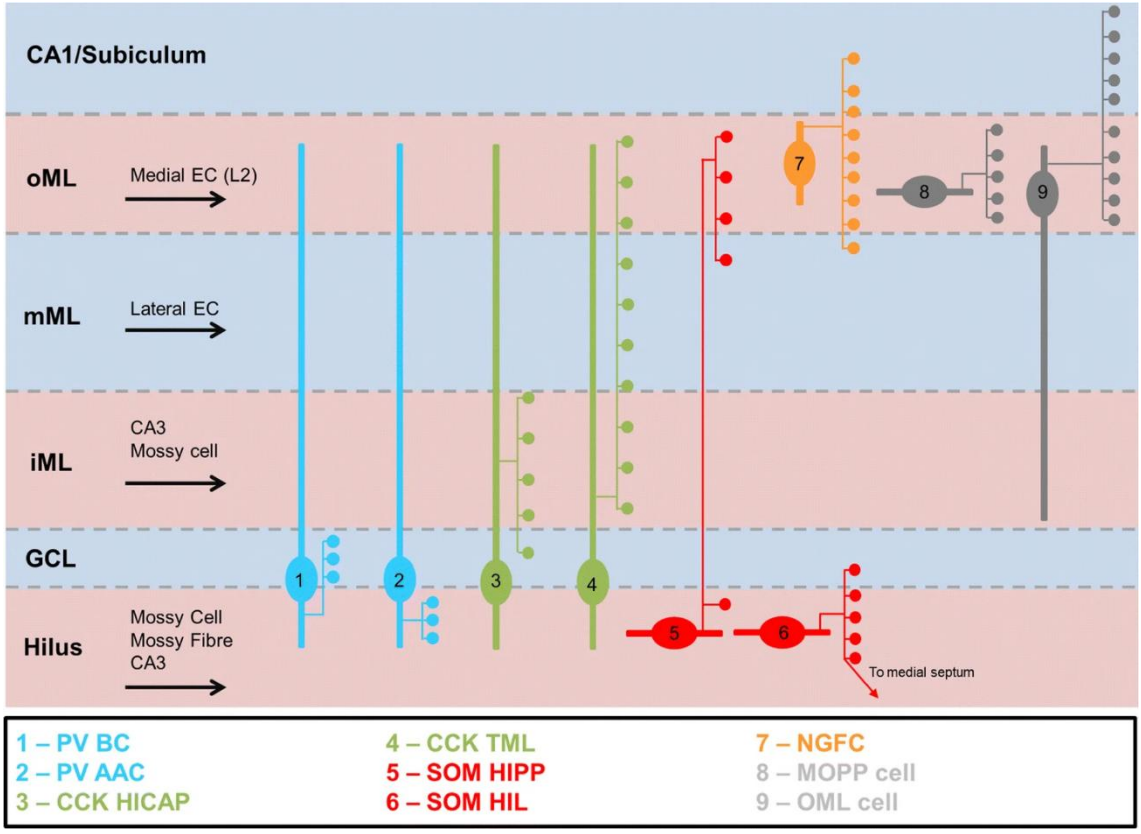


**Figure 3. Schematic representation of the different IN types in the DG.** *A summary of the DG IN types, defined by their neurochemical markers and morphological patterns. Thick lines represent the dendrites and axons. Small circles represent the major areas where their terminals are formed. Colors represent neurochemically defined groups. Abbreviations: HICAP – hilar comissural-associational pathway related cell, TML – total molecular layer cell, HIPP - hilar perforant path-associated cell, HIL – hilar cell, NGFC – neurogliaform cell, MOPP – molecular layer perforant path-associated cell, OML – outer molecular layer cell, oML – outer molecular layer, mML – medial molecular layer, iML – inner molecular layer, GCL – granule cell layer. Source*: [41] , *modified.*

### 1.4.1 Dendrite-targeting interneurons in the hippocampus proper

The dendrite-targeting INs show great morphological variety, and their axon terminals often occupy dendritic segments targeted by distinct excitatory pathways (**Fig. 2**). For example, two representatives of the dendrite-targeting INs in the hippocampus proper are the *Oriens – Lacunosum-Moleculare* (O-LM) cells and the bistratified cells.

The O-LM cells innervate the distal apical dendrites of the PYRs in the *str. lacunosum-moleculare*, where the CA1 PYR dendrites receive TA inputs from the EC [6,42–44].

Meanwhile, the bistratified cells innervate more proximal segments of the CA1 PYR dendrites in the *strata oriens* and *radiatum* where the Schaffer collaterals of CA3 PYRs terminate as well.

This projection pattern indicates that these two populations of INs are inhibiting CA1 PYR dendritic segments that receive excitation from the EC and CA3, respectively. Thus, these INs are in position to inhibit dendritic segments receiving specific inputs.

In the CA1, the dendrites of O-LM INs can be found in the *str. oriens*, where they receive inputs from the CA1 PYR [6,34,45]. In contrast, bistratified cells have dendrites in the strata oriens and radiatum, thus, they can be innervated by both CA3 and CA1 PYRs.

### 1.4.2 Dendrite-targeting interneurons in the dentate gyrus

In the DG, examples of the dendrite-targeting INs are the hilar perforant path-associated (HIPP), hilar (HIL), hilar commissural-associational pathway related (HICAP) and the molecular layer perforant path-associated (MOPP) cells (**Fig. 3**). With the exception of MOPP cells, the somata and dendrites of these GABAergic cells are located in the hilus [6].

The HIPP cells innervate the apical dendrites of the GCs. Similarly to the O-LM cells regarding the CA1 PYRs, these INs are in a perfect position to control the perforant path inputs to the DG GCs. Although their main targets are GCs, results show that these neurons also give synapses to other INs (though to a lesser number). They receive their primary excitatory input from the GCs.

The HIL cells provide fast GABAergic inhibition to PV+ and SOM+ INs alike in the hilus. Apart from the GCs the HIL cells receive excitatory inputs from other sources as well, most probably from MCs. For the sake of simplicity here I mentioned the HIL cells among the INs, however, importantly, recent studies show their long-range connections with the medial septum. This allows them to coordinate the DG activity with the septum-generated theta oscillations [46].

The HICAP cells send their axons to the inner molecular layer where the commissural and associational projections are terminating on the dentate GCs. HICAP cells receive most of their inputs from the GCs [47] .

The MOPP cells are exceptions in that their somata located in the molecular layer. Their axons innervate GC dendrites in the outer molecular layer. Their dendritic tree also arborize in the molecular layer and receive inputs from the perforant path [6,48,49] .

### 1.4.3 Perisomatic region-targeting interneurons in the hippocampus proper

Perisomatic inhibition is provided by axo-axonic cells (AACs) and basket cells (BCs) in the hippocampus (**Fig. 2**). The AACs exclusively innervate the axon initial segments (AIS) of the PCs, while the BCs form synapses on their proximal dendrites and somata. These INs exert strong control over the spiking activity of their postsynaptic partners [34,38,39,50,51].

In the hippocampus proper the cell bodies of the perisomatic region-targeting INs are located in *str. pyramidale* or in *str. radiatum*. They send smooth, radially oriented apical dendrites through the *str. radiatum*, while their basal dendrites arborize in the *str. oriens*.

The axon clouds of the AACs elaborate in the *strata pyramidale* and *oriens* where they innervate the AIS of the PYRs forming characteristic cartridge-like profiles. The BC axons localize in the *strata pyramidale* and *oriens* and form synapses on the somata and proximal dendrites of the PYRs**.**

Hippocampal AACs receive a wide range of inputs for example from the EC, medial septum and the local collaterals of the PYRs [6,52,53]. BCs are also innervated by multiple sources: the mossy fibers in the CA3, the Schaffer collaterals, the commissural pathway, the EC, and local axon collaterals of the PYRs [6] .

### 1.4.4 Perisomatic region-targeting interneurons in the dentate gyrus

In the DG, the somata of the perisomatic region-targeting INs are located in or near the border of the *str. granulosum*.

Both the AACs and BCs give rise to smooth dendrites that arborize mainly in the *str. moleculare* and to a lesser extent give branches to the hilus. An exception is a group of basket cells that only have dendrites in the hilus. The dense axon arborizations of both AACs and BCs are mostly localized in the *str. granulosum*, where the AACs innervate the AISs, while the BCs target the somata and proximal dendrites of the GCs.

In the DG, BCs receive inputs from the commissural-associational fibers, the ipsilateral CA3 and from the perforant path. The AACs also receive inputs from the perforant path and commissural fibers [6,54].

There are still open questions about the inputs of these neurons in the DG. A circuit motif that is present in other cortical areas [55–59] is the presence of perisomatic excitatory synapses on PV-IRs. In the DG, excitatory synapses have been described on the perisomatic region of these INs, however their source has remained unknown [59] .

### 1.5 Excitatory neurons of the dentate gyrus

Similarly to the GABAergic INs, excitatory cell populations are distinguished based on morphological, physiological, developmental, and functional characteristics. The DG has three populations of excitatory neurons: the MCs, the GCs, and the semilunar granule cells (SGCs).

#### 1.5.1 Mossy cells

MCs are the only excitatory cells in the hilus. Their thick, brushy dendrites arborize in the hilus where they receive inputs from GCs, SGCs, other MCs, hilar INs and backprojecting CA3 PYRs [60–63]. MCs also receive long-range inputs from the medial septum and the septofimbrial nucleus. Their axons project both to the ipsilateral and to the contralateral hippocampus. Another characteristic of the MC axons is their long projections along the septotemporal axis of the DG [60].

Some results suggest that the MCs are excitatory feedback neurons: they project back to the GCs that also give rise to their main excitatory inputs [64,65]. Important to note, that *in vivo* studies could not verify the presence of functional monosynaptic connection from MCs to GCs [66]. Due to their large somata, thick dendrites and long axons, in extracellular electrophysiological recordings the activity of a single MC can be picked up from as far as 300 microns. Previously, this made their identification in these recordings

difficult since in the past it relied mostly on the localization of the recording electrodes. Recent results, however, show a combination of features that allow reliable identification of MCs in *in vivo* extracellular recordings [66].

Despite these advancements, the role of MCs in neural computations and different behaviors is still an open question. One theory is the GC associational hypothesis [67,68] . This posits that MCs sample and distribute information in large networks of GCs. Thus, a main role of MCs could be to connect GC assemblies and serve as local circuit integrators during associative memory formation.

MCs also serve as a first step in processing the backpropagating activity of the CA3 PCs. As they project to long distances along the septotemporal axis of the DG and innervate many GCs and INs, they are able to efficiently connect the CA3 PCs networks to the DG. In line with this, *in vitro* recordings show that during sharp-wave ripples they reliably receive excitatory and inhibitory postsynaptic currents (EPSCs and IPSCs, respectively). Additionally, around 50% of the MCs increase their firing activity following the sharp-wave ripples with a ~6.4 ms delay. Upon the increase in firing of the MCs, GCs also increase their activity and SWR-related EPSCs in GCs lagged with a ~4.2 ms behind those detected in MCs, suggesting that sharp-wave ripple activity backpropagates to the GCs from the CA3 through the MCs in a disynaptic manner [69]

It has also been shown that MCs play a role in spatial information processing. While only a very low proportion of recorded GCs tend to show position specific activation (place field) in a given environment, MCs frequently have multiple place fields [66,70] . Results also show that MCs play a role not only in spatial coding but also in spatial memory formation [71]. These results are in line with the impairment of spatial navigation in temporal lobe epilepsy patients in whom MC (and other neurons, such as CA1 PYR) loss occurs [71,72].

### 1.5.2 Granule cells

The GCs are the PCs of the DG. Their small (10 µm in diameter) somata are densely packed in the *str. granulosum* [7,73]. These cells are monopolar in rodents with their characteristic, cone-shaped apical dendrites bifurcating close to the soma and spanning the molecular layer.

The GC axons form the mossy fibers that enter the hilus and project to the CA3. In the hilus, the mossy fibers form synapses on the proximal dendrites of MCs at so-called thorny excrescences, whereas INs are innervated via simple, small varicosities. A marker utilized in neuroanatomical studies for identifying GC terminals is their high levels of $Zn^{2+}$, for example, detected by the Timm-staining [59].

In the CA3, similarly to the hilus, the mossy fibers form small boutons on the INs and large mossy terminals with multiple active zones on the proximal dendrites of the CA3 PYRs [17,74]. Another example of the mechanisms through pattern separation is achieved is the markedly different operation of these two types of terminals. The mossy terminals have a low initial release probability and show strong facilitation. In contrast, the small boutons the GCs form on INs have a high initial release probability but show no facilitation [75].

As GCs have a hyperpolarized membrane potential, normally they sparingly (~1 Hz) fire single action potentials (APs). However, upon receiving excitation they tend to fire 3-7 AP in a short burst (10 Hz). A single AP is not enough to activate the CA3 PYRs due to the low initial release probability of the mossy terminals, but enough to activate the INs.

Thus, GCs activate feed-forward inhibition in the CA3 network during their single AP firing mode. Meanwhile, those GCs that receive substantial excitation are activated and start firing bursts of APs. Through the facilitation of the mossy terminals these bursts reliably activate the postsynaptic PYRs. This elegant mechanism lets the GCs to activate the CA3 PYRs in a strictly controlled and shaped manner, thus allowing the DG networks to transmit the orthogonal activity patterns it isolated from the multimodal cortical inputs during pattern separation [76].

### 1.5.3 Semilunar granule cells

The SGCs have been suggested to form a subtype of GCs. The cell bodies of the SGCs are mainly located in the GCL. In contrast to the GCs however, SGC somata always sit close to the *str. granulosum – str. moleculare* border or sometimes even in the *str. moleculare* and show a preference for the suprapyramidal blade [77]. Contrary to GCs, SGCs are multipolar, their dendritic tree is more widely expanding and their axons extend collaterals within the *str. granulosum*. Similarly to the GCs, SGC terminals also contain high levels of zinc [59].

In terms of physiology, similarly to the GCs, they have relatively negative resting membrane potential and fire overshooting APs. However, the SGCs have several physiological features that set them apart from GCs. They show a depolarization ramp before each AP and a long afterhyperpolarization. Moreover, upon receiving a longer (2 s) depolarizing current step the GCs fire APs only during the first 50-100 ms, while the SGCs fire throughout the current step. This allows SGCs to have a longer time window for synaptic integration compared to the GCs and suggests they fulfil a special function in the DG that markedly differs from the GCs [78].

Results gained using *in utero* virus injections also pointed out that SGCs tend to born earlier, around the E12-E14 days during the embryonic development, while GCs tend to born later [79]. At the behavioral level SGCs proposed to be preferentially activated during encoding novel stimuli and environments [77].

These results together indicate that SGCs differ from GCs in anatomical, physiological, developmental and functional features underlying that these neurons form a distinct subtype of the dentate GCs.

However, little is known about how the SGCs integrate into the DG circuitry. Like the GCs they receive excitatory synapses from the hilar MCs and receive EPSPs with similar kinetics to the GCs from the perforant path. It has also been shown that SGCs axons innervate hilar MCs and INs, and project to the CA3 [80–82].

Previous results show that the perisomatic region of PV-IRs in the DG are heavily contacted by $Zn^{2+}$-containing boutons [59]. The source of this input was not known and has been assumed to be the GCs, although, they do not send axonal collaterals to the str. granulosum, where many PV-IRs are present. Thus, SGCs may be a probable source for the perisomatic excitation of PV-IRs in the DG. Therefore, in our work presented in the first part of my dissertation, we aimed to test the hypothesis that SGCs provide the perisomatic excitation to the DG PV-IRs.

### 1.6 Relevance of TRPC6 channels

Ion channels are fundamental in neuronal computations. In animals, there are hundreds of ion channel genes [83]. The orchestrated cellular and subcellular expression patterns

of these diverse molecules are necessary for the functioning of neural circuits. Learning the precise cellular and subcellular distribution of these channels on the highly polarized neurons greatly facilitates our understanding of their possible functions.

In the second part of my dissertation, I will present our work focusing on the cellular and subcellular distribution of TRPC6 channels in the hippocampus. These channels proposed to be involved in several hippocampal functions. Moreover, possibly these channels are also part of the endocannabinoid signaling pathway further highlighting their potential role in hippocampal computations.

The TRPC6 channels are transient receptor potential (TRP) channels, which are a conserved group of cation channels. These are intrinsic membrane proteins, built up by 6 transmembrane helices with the N- and C-terminals on the intracellular side [84,85]. The TRP superfamily is divided into 7 families (TRPC, TRPV, TRPM, TRPN, TRPA, TRPP and TRPML) based on sequence homology [86,87]. In mammals the "canonical" TRP channels form the TRPC subfamily, which shows the largest homology with the TRP channels in the Drosophila. There are 7 different TRPC channels (TRPC1-7). The TRPC6 channels are non-selective cation channels with a relatively high permeability for $Ca^{2+}$ ions ($PCa^{2+}/PNa^{+}$ – 5:1) [88]. TRPC6 channels are expressed both in neuronal and non-neuronal tissue. In the brain TRPC6 channels are present only in a few regions, such as the hippocampus or the cerebellum and they are involved in several physiological and pathological phenomena for example in spatial navigation, synapse formation, or epilepsy [89,90].

A specific activator of TRPC6 channels is hyperforin, the active constituent of the Hypericum perforatum (St. John's wort) extract [91,92]. It has been shown that hyperforin has an antidepressant effect in mild and moderate depression. In line with this, in an elevated plus maze Trpc6 knockout (KO) mice tend to explore less in the open arm (however in the marble burying test show no signs of increased anxiety) [93].

TRPC6 is also involved in hippocampal-dependent spatial memory functions. TRPC6 overexpression leads to improved spatial memory in Morris water maze test. Moreover, hyperforin also rescued spatial memory impairments in several behavioral tests such as the Morris water maze test, open field test, active – and passive avoidance tasks pointing to the role of TRPC6 receptors in these behaviors [90]. TRPC6 channels have been also

shown to be involved in forming and maintaining excitatory synapses on hippocampal spines [94,95].

All the abovementioned phenomena are linked to the hippocampus, highlighting the functional role of TRPC6 channels in the hippocampal circuitry. Therefore, in order to understand how TRPC6 channels could contribute to physiological and pathological neural computations in the hippocampus, our aim was to determine which exact neural elements of the hippocampus express these channels.

### 1.7 Physiological activation of TRPC6 channels

TRPC6 channels can be activated through multiple other mechanisms. Phospholipase C is activated by several G-protein coupled receptors, such as mGluR1/5 and receptor tyrosine kinases, such as the TrkB receptors. PLC hydrolyzes phosphoinositol-diphosphate-2 (PIP2) into diacylglycerol (DAG) and inositol-triphosphate-3 (IP3). The IP3 can bind to its receptors on smooth endoplasmic reticulum, which serve as intracellular $Ca^{2+}$-stores. The depleted $Ca^{2+}$-levels of the ER activate STIM2, which in turn could activate the TRPC6 channels [90,96] . Meanwhile, the hydrophobic DAG remains in the membrane and can directly activate TRPC6 receptors. DAG also acts on several other effectors such as the DAG-lipase. DAG-lipase hydrolyzes DAG in a $Ca^{2+}$-dependent manner [97] and produces an endocannabinoid secondary messenger, the 2-arachidonoylglycerol (2-AG) [98].

DAG-lipase, mGluR1/5 and PLC are all has been shown to be present in excitatory synapses closely localized to each other in the perisynaptic zone in the hippocampus [99–103]. Therefore, in order to understand if the TRPC6 channels could be part of this signalization pathway [104], we also aimed to precisely determine the subcellular distribution of TRPC6 channels in the hippocampus.

## 2. OBJECTIVES

The aims of this PhD dissertation were:

I/

1. Reveal the source of the perisomatic asymmetric synapses on the PV-IRs in the DG.

II/

1. Provide an overview of the expression of TRPC6 channels in the hippocampus of WT mice and rats and confirm the specificity of the TRPC6 antibody used in this study using Trpc6 KO mice
2. Determine which neuronal elements of the hippocampus express TRPC6 channels in rats and mice.
3. Investigate the density of TRPC6 channels in different compartments of the DG GCs.
4. Determine the distribution of TRPC6 channels on the dendritic spines of the DG GCs.
5. Determine the subcellular localization of TRPC6 channels in the mossy fibers and mossy terminals.
6. Identify the IN populations in the hippocampus that expresses TRPC6 channels.
7. Determine the subcellular localization of TRPC6 channels in IN dendrites.

# 3. METHODS

## 3.1 Source of perisomatic excitation on parvalbumin-immunoreactive interneurons in the dentate gyrus

The methods and materials used to determine the source of perisomatic excitation on PV-IRs in the DG have been described in: [105].

### Animals

CD-1 ICR mice (Harlan) were used in this study. 3 to 6 mice were housed together under a 12/12h light/dark cycle. Food and water were available ad libitum. Animals were habituated to the animal facility for a minimum of 2 days before the experiments. Handling was minimized to avoid unnecessary stress for the mice. All procedures were conducted in accordance with Directive 2010/63/EU of the European Parliament and of the European Council of 22 September 2010 on the protection of animals used for scientific purposes.

The mice used in this study for anatomical investigations were between 2 and 5 months old. Both female and male mice were used. Data from female and male mice were not analyzed separately, because there was no evidence regarding the anatomical differences in the expression of studied cell markers or in the studied projections. For anatomical investigations mice were deeply anesthetized using pentobarbital. Next, transcardial perfusion was performed first with 10 ml of saline which was followed by fixative for 30 minutes at a flow rate of 4 ml/min. For wide-field light microscopy and confocal microscopy investigations, the fixative consisted of 4% paraformaldehyde (PFA) with 15% of a saturated solution of picric acid in 0.1 M phosphate buffer (PB). For electron microscopy, the same fixative additionally contained 0.5% glutaraldehyde. For Timm-staining, animals were initially perfused with 20 ml of 0.05% $Na_2S$ in PB instead of saline (at a flow rate of 4 ml/min), followed by the fixative used for light microscopy. After perfusion, brains were removed and 60-µm-thick sections were prepared using a vibratome (VT1000S, Leica). All tissue was stored in PB containing 0.05% sodium azide at 4°C.

Fluorescent immunohistochemistry

The immunostainings for confocal microscopy were performed on free-floating sections. The sections were blocked for 1 hour at room temperature in 10% normal donkey serum (NDS) prepared in PB saline containing 0.2% Triton X-100 (PBS-Tx). Incubations with primary antibodies were performed either overnight at room temperature or for 48 hours at 4°C. The following primary antibodies were used: guinea pig anti-parvalbumin (1:2000; 195004 Synaptic Systems), rabbit anti-parvalbumin (1:5000; PV-28 Swant). The secondary antibodies (1:400) were donkey anti-rabbit IgG conjugated with Alexa Fluor 488 (Invitrogen); goat anti-guinea pig IgG conjugated with Alexa Fluor 488 (Invitrogen). Following the immunostainings, sections were mounted on slides using Mounting Medium for fluorescence (refractive index 1.47–1.5; DAKO). Slides were evaluated using a confocal scanning microscope (Leica TSC-SPE).

Immunohistochemistry for electron microscopy

For electron microscopy, sections from animals fixed with glutaraldehyde-containing fixative were used. To enhance antiserum penetration, the sections first were cryoprotected in 10% glycerol and 25% sucrose in 0.01 M PB. Then the sections were freeze-thawed three times above liquid nitrogen. No detergent was used during washing or incubation. Sections were then treated with 1% sodium borohydride in 0.1 M PB for 20 min and blocked in 10% normal goat serum prepared in 0.1 M PB. Next, immunostaining was performed using rabbit anti-parvalbumin (1:5000; PV-28 Swant), biotinylated goat anti-rabbit IgG (1:200; Invitrogen), and ABC (1:200; DAKO), followed by diaminobenzidine (DAB) development to produce a brown reaction product. Sections were then treated with 1% OsO4 (Electron Microscopy Sciences) and 7% glucose in 0.1 M PB for 45 minutes at room temperature, followed by treatment with 2% uranyl acetate in maleate buffer. Sections were subsequently dehydrated in an ascending series of cold ethanol, cleared in propylene oxide, embedded in epoxy resin (Durcupan, Sigma), and flat mounted on microscope slides. Specimens were first examined by light microscopy, and cells selected for electron microscopy were isolated and re-embedded in epoxy resin blocks. Ultrathin sections (50-nm-thick) were cut using an ultramicrotome (Leica EM UC6), collected on Formvar-coated grids, and counterstained with lead citrate for

12 minutes. Ultrathin sections were examined using a JEOL JEM-1010 transmission electron microscope. Images were acquired with either a MegaView I digital camera or an AMT RX80 digital camera.

Synaptic zinc histochemistry

In case of the zinc histochemistry, specimens were processed immediately for Timm-staining to minimize loss of zincergic fibers. As described above, these mice were transcardially perfused first with 20 ml of 0.05% $Na_2S$ in PB instead of saline, which was followed by the fixative used for light microscopy. Following removal of the brains, 60-µm-thick sections were prepared using a vibratome. The sections were washed 3 × 20 minutes in 0.1 M PB and then incubated in a solution containing 14% acacia gum, 1.7% hydroquinone, 0.08% silver nitrate, 2.4% citric acid, and 2.3% trisodium citrate. Autometallography was terminated with 5% sodium thiosulfate in PB. Sections were then either processed for immunohistochemistry against parvalbumin (rabbit anti-parvalbumin, 1:5000; PV-28 Swant) using the ABC method or mounted directly.

Whole-cell patch-clamp

For whole-cell patch-clamp recordings CD-1 mice at postnatal days 15-23 were used. This age range was selected because it provided high cell survival during slice preparation while preserving a relatively well-formed DG and maintaining the health of the possible postsynaptic PV-IRs. For preparation of acute in vitro slices pups were deeply anesthetized with isoflurane (IsoFlo 1385 ESP, Esteve Veterinaria) and decapitated. The head was immediately transferred to an ice-cold solution containing 2.5 mM KCl, 5 mM $MgCl_2$, 0.5 mM $CaCl_2$, 1.25 mM $NaH_2PO_4$, 10 mM glucose, 26 mM $NaHCO_3$, and 252 mM sucrose, bubbled with carbogen (95% $O_2$/5% $CO_2$), and the brain was rapidly removed from the skull. Horizontal slices of 300-µm thickness were cut with a vibratome (VT 1000S, Leica) and transferred to an interface-type holding chamber containing artificial CSF (aCSF) at room temperature. The aCSF contained 2.5 mM KCl, 2 mM $MgCl_2$, 2 mM $CaCl_2$, 1.25 $NaH_2PO_4$ mM, 10 mM glucose, 26 mM $NaHCO_3$, and 126 mM NaCl, bubbled with carbogen. Slices were allowed to stabilize in this solution for at least

1 hour before transferring them to the recording chamber. Patch pipettes were pulled from borosilicate glass capillaries with an outer diameter of 1.5 mm and an inner diameter of 0.84 mm (World Precision Instruments) using a P-97 puller (Sutter Instruments). Pipettes were filled with a solution containing 4 mM NaCl, 110 mM K-gluconate, 20 mM KCl, 10 mM HEPES, and 2 mM $MgCl_2$. Biocytin (Sigma) was added to the solution for intracellular labeling of recorded cells. Pipette resistance, measured in the bath, ranged from 3 to 6 MΩ. Recordings were obtained in oxygenated aCSF under visual guidance using an Olympus microscope (BX51WI, Olympus) equipped with differential interference contrast optics and a NIR CCD camera (C7500-51 Hamamatsu). Signals were recorded with an AM2400 amplifier (AM Systems) connected to a CED Micro 1401 AD converter (Cambridge Electronic Design Limited). Recorded neurons were kept for 5 minutes in voltage clamp at a holding voltage of −75 mV, consistent with previous reports indicating that these cells have a hyperpolarized resting membrane potential [78,106–108]. Patched cells were driven to fire APs for at least 10 minutes to improve axonal filling. After 10–20 minutes, slices were fixed by immersion using fixative containing 4% PFA and 0.5% glutaraldehyde. Fixed slices were re-sectioned to 60-µm-thick sections and processed for biocytin detection using ABC (1:200, 4 h). The reaction was visualized with Ni-intensified DAB (DAB-Ni). Cells displaying collaterals with varicosities in the inner molecular layer and granule cell layer were processed for parvalbumin immunoreactivity (rabbit anti-parvalbumin, 1:5000; PV-28 Swant) using DAB, for either light microscopy or electron microscopy as described above. A subset of fixed slices was developed with Alexa Fluor 488-conjugated streptavidin (1:400; Molecular Probes S11223) in PB containing 0.2% Triton X-100, mounted in DAKO fluorescent mounting medium, and imaged with a confocal scanning microscope (Leica TSC-SPE, HCX PL APO U-V-I 40× objective; NA: 0.75, Z step size 0.84 µm, xy: 0.27 µm/pixel). After imaging, slices containing collaterals with varicosities in the *str. granulosum* were demounted, re-sectioned to 60-µm-thick sections, developed with DAB-Ni, and processed for parvalbumin immunoreactivity as described above. An additional batch of slices was developed with Cy3-conjugated streptavidin (1:5000; Sigma-Aldrich S6402) in PB containing 0.5% Triton X-100 and subsequently immunostained for parvalbumin [rabbit anti-parvalbumin (1:1000; SySy 195002) in PB

containing 1% Triton X-100], followed by visualization with an A488-conjugated donkey anti-rabbit antibody (1:400; Jackson 711545152).

### Morphometric analysis of GCs and SGCs

Morphological differences between the two populations of GCs were assessed using confocal stacks of intracellularly filled cells visualized with Streptavidin-A488 or Streptavidin-Cy3. Sholl analysis of the dendritic arbor was performed [109] using the Stitching plugin and the Simple Neurite Tracer plugin in ImageJ. The number of primary dendrites, dendritic spread angle (considering a vertex the most basal part of the soma and the sides as the most lateral dendrites in the outer molecular layer), total dendritic length, and horizontal soma diameter were also evaluated.

### Statistical analysis

Statistical analyses were performed using OriginPro2015. Comparison of the morphometric analyses were done using the Mann–Whitney test. Graphs were prepared using OriginPro 2015. Data are presented as mean ± SEM.

## 3.2 Subcellular distribution of TRPC6 channels

The methods and materials used to determine the subcellular distribution of TRPC6 channels have been described in [110].

### Animals

Experiments were performed according to the guidelines of the Institutional Ethical Codex and the Hungarian Act of Animal Care and Experimentation (1998, XXVIII, section 243/1998), which conforms to the regulations of animal experiments of the European Union. All animals were housed in a 12h-12h light-dark cycle with water and food available ad libitum. All efforts were made to minimize pain and suffering and to reduce the number of animals used. In this study, 10 male Wistar rats (200–400 g; Charles

River, Hungary) and two adult Trpc6 KO mice and their wild type (WT) littermates (n = 2) were used.

Immunohistochemistry

Rats were deeply anesthetized with equitesin administered intraperitoneally (4.2% wt/vol chloral hydrate, 2.12% wt/vol $MgSO_4$, 16.2% wt/wt Nembutal, 39.6% wt/wt propylene glycol, and 10% wt/wt ethanol in $H_2O$) at a dosage of 0.2 ml/100 g body weight. Transcardial perfusion was performed sequentially with 4°C 0.9% NaCl for 2 minutes, followed by a fixative containing 2% PFA and 3.75% Acrolein in 0.1 M phosphate buffer (PB; pH = 7.4) for 10 minutes, and then a fixative containing 2% PFA in 0.1 M PB for 20 minutes. Mouse brains were fixed by immersion in 4% PFA. Coronal sections of 40–50 μm in thickness were cut using a Leica 1000S vibratome, cryoprotected overnight in 30% sucrose in 0.1 M PB, and freeze thawed in an aluminum foil boat over liquid nitrogen to improve antibody penetration. After washing, the sections were incubated for 10 minutes in 0.1 M PB containing 1% sodium borohydride.

Then sections then were placed for 30 minutes to a solution containing 2% bovine serum albumin (BSA), 100 mg/ml glycine, and 10% normal goat serum (Vector laboratories) in Tris-buffered saline (TBS), pH 7.4. This was followed by incubation overnight at 4°C with a rabbit anti-TRPC6 antibody (Alomone Labs Ltd, Jerusalem, Israel) diluted 1:20,000 in TBS. After washing out the primary antibody, the sections were incubated in a biotinylated goat-anti rabbit secondary antiserum (Vector Laboratories, Burlingame, CA) diluted 1:200 in TBS for 2 hours Sections were then treated with a solution containing avidin-biotinylated horseradish peroxidase complex (ABC Elite, Vector Laboratories) 1:300 in TBS for 2 hours followed by immunoperoxidase reaction using DAB (Sigma-Aldrich, St Louis, MO) as a chromogen.

To determine the subcellular localization of TRPC6, pre-embedding immunogold staining was used. In these experiments, the sections were incubated in the anti-TRPC6 antiserum (1:5000) for 2 days, followed by application overnight of a 1 nm gold-conjugated anti-rabbit secondary antibody (Aurion, Wageningen, The Netherlands) diluted 1:50 in TBS containing 1% BSA, 0.1% fish gelatine, and 100 mg/ml glycine. The

sections were then postfixed in 2% glutaraldehyde in TBS and silver intensified with the Aurion R-Gent silver intensification kit.

All immunoperoxidase- and immunogold-stained sections were treated in 0.5% $OsO_4$ for 1 minute, then in 1% $OsO_4$ for 15 minutes in 0.1 M PB followed by dehydration in an ascending alcohol series and acetonitrile and embedded in Durcupan. During dehydration, the sections were treated with 1% uranyl acetate in 70% ethanol for 30 minutes. Finally, sections were re-embedded and examined with a light (Zeiss Axioscope 2) or an electron microscope (JEOL, JEM-1011).

For confocal laser microscopy, a mixture of primary antisera of anti-TRPC6 (1:3000) and guinea pig anti-mGlu1a (1:500; Frontier Institute co. Ltd, Japan; [111] or anti-TRPC6 (1:3000) and mouse anti-parvalbumin (1:2000; Sigma-Aldrich) was used. The sections were then incubated for 2 hours with a mixture of secondary antibodies diluted in TBS: Alexa Fluor 488 goat anti-rabbit antibody (1:200, Molecular Probes, Eugene, OR) and Alexa Fluor 594 goat anti-guinea pig (1:200, Molecular Probes), or Alexa Fluor 488 goat anti-rabbit antibody (1:200, Molecular Probes) and Alexa Fluor 594 goat anti-mouse (1:200, Molecular Probes). After washing, the sections were mounted on glass slides and covered in Aqua poly/mount (Polysciences, Warrington, PA). Coverslips were sealed in nail polish. Images were taken with a Nikon A1R confocal laser scanning microscope using a sequential scanning mode.

Quantitative analysis of the distribution of TPRC6 channels in dentate granule cells

All quantifications were carried out on tissue samples derived from three rats. For analysis using ImageJ software (NIH), silver-intensified immunogold particles located <100 nm from the cell membrane were counted as plasma membrane-attached. Images were taken from three sequential ultrathin sections (cut using a Leica ultramicrotome) in the middle part of the *str. moleculare* or *str. granulosum* at a magnification of ×2,500. Calculation of particle density was performed on the central image, in which all profiles were identified as spine, dendrite, soma, axon ending, or unknown profile using the two adjacent images. The number of gold particles divided by the total length of the membranes was calculated for all those dendrites, spines, and somata measured in the

central image whose profiles were not truncated by the edge of the image. Since the distributions of immunogold labeling calculated on each image were not different from normal distributions ($p > 0.05$, Shapiro-Wilk test), the mean and standard error of the mean (SEM) of membrane-associated immunogold particles per 1 μm of the plasma membrane were used to describe the distributions of immunolabeling in each compartment (dendrites, spines and cell bodies).

To determine the distribution of TRPC6 labeling in spine heads, 93 immunogold particles were counted from each animal ($n = 3$). Using an approach comparable to that published previously [99,100], the distance of each immunogold particle was measured along the plasma membrane from the edge of the synaptic junction for each immunogold particle and the data were divided into 60 nm bins. The three datasets were not different from each other ($p > 0.5$, Kruskal–Wallis non-parametric test), so the data were pooled.

## 4.1 RESULTS – I.

### 4.1.1 Perisomatic excitatory innervation from Timm-positive boutons on parvalbumin-immunoreactive interneurons in the granule cell layer

Previous studies using Timm-staining showed that $Zn^{2+}$-containing terminals innervate the perisomatic region of the PV-IRs [59]. Since the Timm-staining only labels the axon varicosities it does not give information about the neurons that give rise to these terminals. However, based on the $Zn^{2+}$-content and morphology of these terminals it was hypothesized that GCs or SGCs might give rise partially or entirely to these excitatory inputs. As these studies were performed in rats, to confirm the presence of this innervation in mice, first we combined the Timm-staining with parvalbumin-staining in mice. Our results show, that similarly to rats, in mice Timm-positive boutons formed basket-like profiles around PV-IR somata in the DG [59,105,112,113] **(Fig. 4A**).

### 4.1.2 Typical granule cells do not have axon collaterals in the granule cell layer

Next, to identify the source of the Timm-positive innervation on PV-IRs, we intracellularly filled GCs and SGCs with biocytin **(Fig. 4B)**.

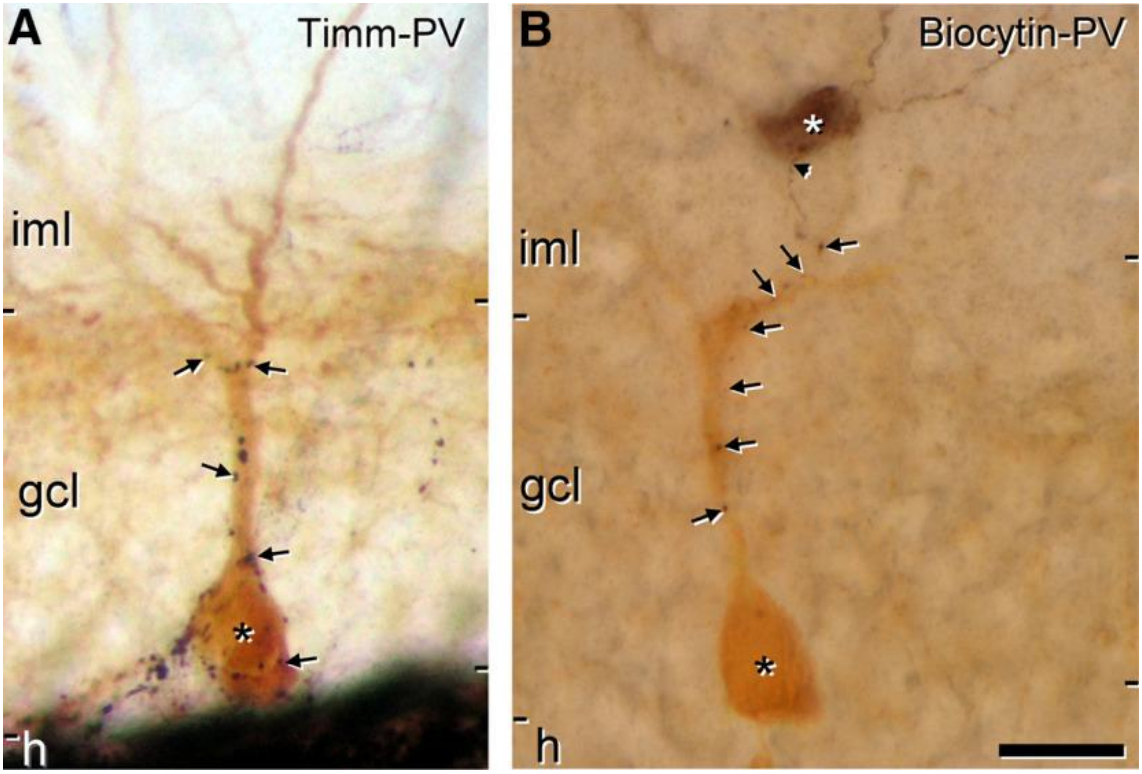


***Figure 4. SGCs form close appositions on PV-IRs resembling the innervation by Timm-stained boutons.*** ***A****, Timm-stained boutons (arrows) form close appositions on a PV-IR (asterisk) in the granule cell layer. Note that Timm-staining only reveals the axonal varicosities, thus the origin of them cannot be resolved. The image was reconstructed from several optical planes.* ***B****, An intracellularly filled SGC (white asterisk) in the inner molecular layer gives rise to an axon (arrowhead) that forms close appositions (arrows) on a PV-IR (black asterisk). Abbreviations: gcl, granule cell layer; h, hilus; iml, inner molecular layer; oml, outer molecular layer. Scale bar: 20 µm. Source:* [105]

Then, in order to separate SGCs and GCs from each other, we analyzed their morphological differences. In accordance with previous results [78,79] by performing Sholl analysis on the morphological features, we found several differences. The number of intersections up to the first 60 microns from the soma, the number of the primary dendrites, the spread angle of the dendritic angle, the total dendritic length and the soma horizontal diameter were all larger in the SGCs than in the GCs (**Table 1)**. These results

show that GCs and SGCs can be separated from each other based on their morphological differences in our dataset [105].

***Table 1. Statistical analysis of the morphologic characteristics of classical GCs, SGCs, and SGC-PVs.*** *(Data are shown as mean ± SEM. For comparison the Mann–Whitney test was used). Source:* [105]

| | GCs | SGCs | SGC-PVs | MW (GCs vs SGCs) | MW (GCs vs SGCs-PV) | MW (SGCs vs SGCs-PV) |
|---|---|---|---|---|---|---|
| Number of primary dendrites | 1.5 ± 0.22 ($n$ = 10) | 4.0 ± 0.32 ($n$ = 18) | 3.75 ± 0.56 ($n$ = 8) | $p < 0.001$ | $p = 0.003$ | $p = 0.797$ |
| Dendritic spread angle (°) | 73.4 ± 8.5 ($n$ = 10) | 120.9 ± 5.0 ($n$ = 18) | 107.3 ± 11.0 ($n$ = 8) | $p < 0.001$ | $p = 0.037$ | $p = 0.389$ |
| Total dendritic length ($\mu$m) | 1575 ± 114 ($n$ = 10) | 2055 ± 103 ($n$ = 20) | 1779 ± 212 ($n$ = 4) | $p = 0.009$ | $p = 0.358$ | $p = 0.296$ |
| Somatic horizontal diameter ($\mu$m) | 11.3 ± 0.59 ($n$ = 10) | 13.6 ± 0.79 ($n$ = 17) | 11.9 ± 1.03 ($n$ = 8) | $p = 0.039$ | $p = 0.894$ | $p = 0.210$ |
| Sholl analysis | | | | | | |
| Intersections at 20 $\mu$m | 2.4 ± 0.52 ($n$ = 10) | 5.55 ± 0.38 ($n$ = 20) | 5.29 ± 0.68 ($n$ = 7) | $p < 0.001$ | $p = 0.010$ | $p = 0.865$ |
| Intersections at 40 $\mu$m | 4.5 ± 0.45 ($n$ = 10) | 7.0 ± 0.33 | 7.43 ± 0.61 ($n$ = 7) | $p < 0.001$ | $p = 0.005$ | $p = 0.571$ |
| Intersections at 60 $\mu$m | 6.3 ± 0.54 ($n$ = 10) | 8.2 ± 0.45 ($n$ = 20) | 8.29 ± 0.80 ($n$ = 7) | $p = 0.022$ | $p = 0.068$ | $p = 0.845$ |
| Intersections at 80 $\mu$m | 8.2 ± 0.80 ($n$ = 10) | 9.1 ± 0.39 ($n$ = 20) | 9.0 ± 1.41 ($n$ = 7) | $p = 0.392$ | $p = 0.730$ | $p = 0.843$ |
| Intersections at 100 $\mu$m | 8.1 ± 0.82 ($n$ = 10) | 9.35 ± 0.54 ($n$ = 20) | 8.86 ± 1.64 ($n$ = 7) | $p = 0.436$ | $p = 0.883$ | $p = 0.285$ |
| Intersections at 120 $\mu$m | 9.2 ± 0.83 ($n$ = 10) | 10.1 ± 0.57 ($n$ = 20) | 9.17 ± 1.99 ($n$ = 6) | $p = 0.463$ | $p = 0.620$ | $p = 0.104$ |
| Intersections at 140 $\mu$m | 8.2 ± 1.33 ($n$ = 10) | 8.65 ± 0.73 ($n$ = 20) | 7.67 ± 1.86 ($n$ = 6) | $p = 0.773$ | $p = 0.785$ | $p = 0.409$ |
| Intersections at 160 $\mu$m | 5.6 ± 1.27 ($n$ = 10) | 6.5 ± 0.67 ($n$ = 20) | 3.83 ± 1.19 ($n$ = 6) | $p = 0.506$ | $p = 0.412$ | $p = 0.061$ |
| Intersections at 180 $\mu$m | 3.5 ± 1.06 ($n$ = 10) | 3.8 ± 0.61 ($n$ = 20) | 2.33 ± 1.23 ($n$ = 6) | $p = 0.876$ | $p = 0.532$ | $p = 0.268$ |
| Intersections at 200 $\mu$m | 1.3 ± 0.54 ($n$ = 10) | 2.2 ± 0.47 ($n$ = 20) | 1.83 ± 0.91 ($n$ = 6) | $p = 0.283$ | $p = 0.727$ | $p = 0.683$ |
| Intersections at 220 $\mu$m | 0.4 ± 0.31 ($n$ = 10) | 1.2 ± 0.28 ($n$ = 20) | 1.0 ± 0.51 ($n$ = 6) | $p = 0.087$ | $p = 0.261$ | $p = 0.846$ |

Examining 19 GCs we found that in line with previous results [17,114], GCs did not give rise to collaterals in the *str. granulosum* and in the DG only formed varicosities in the *hilus*.

4.1.3 Semilunar granule cells give rise to asymmetric synaptic contacts on parvalbumin-immunoreactive interneurons

To determine whether the SGCs give rise to perisomatic excitatory inputs to PV-IRs, we filled intracellularly 41 SGCs with biocytin, re-sectioned them and developed the sections

with DAB-Ni. Subsequent parvalbumin-staining revealed that 4 SGCs gave putative contacts to the perisomatic region of PV-IRs (SGC-PV). These closely resembled to the Timm-positive axon varicosities from earlier results [59] **(Fig. 4B)**.

Additionally, in another batch of biocytin-filled SGCs we performed the parvalbumin staining without re-sectioning and developed the sections with streptavidin-Cy3. In this batch of 47 filled SGCs 4 gave rise to close contacts in the perisomatic region of PV-IRs **(Fig. 5A-D)**. Based on these results, in the DG the source of the perisomatic excitatory innervations of the PV-IRs are not the GCs but the SGCs.

We pooled all the 8 SGC-PVs from these experiments and compared their morphological features to the remaining SGCs and GCs. Sholl-analysis revealed that they were different from the GCs but could not be distinguished from the SGCs. The SGC-PV neurons differed from the GCs in the number of dendritic intersections close to their somata, the number of primary dendrites, the dendritic spread angle, total length of the dendritic tree and the horizontal diameter of the somata. In contrast to this, there were no morphological differences between the SGCs and SGC-PVs [105] (**Fig. 5E-I**).

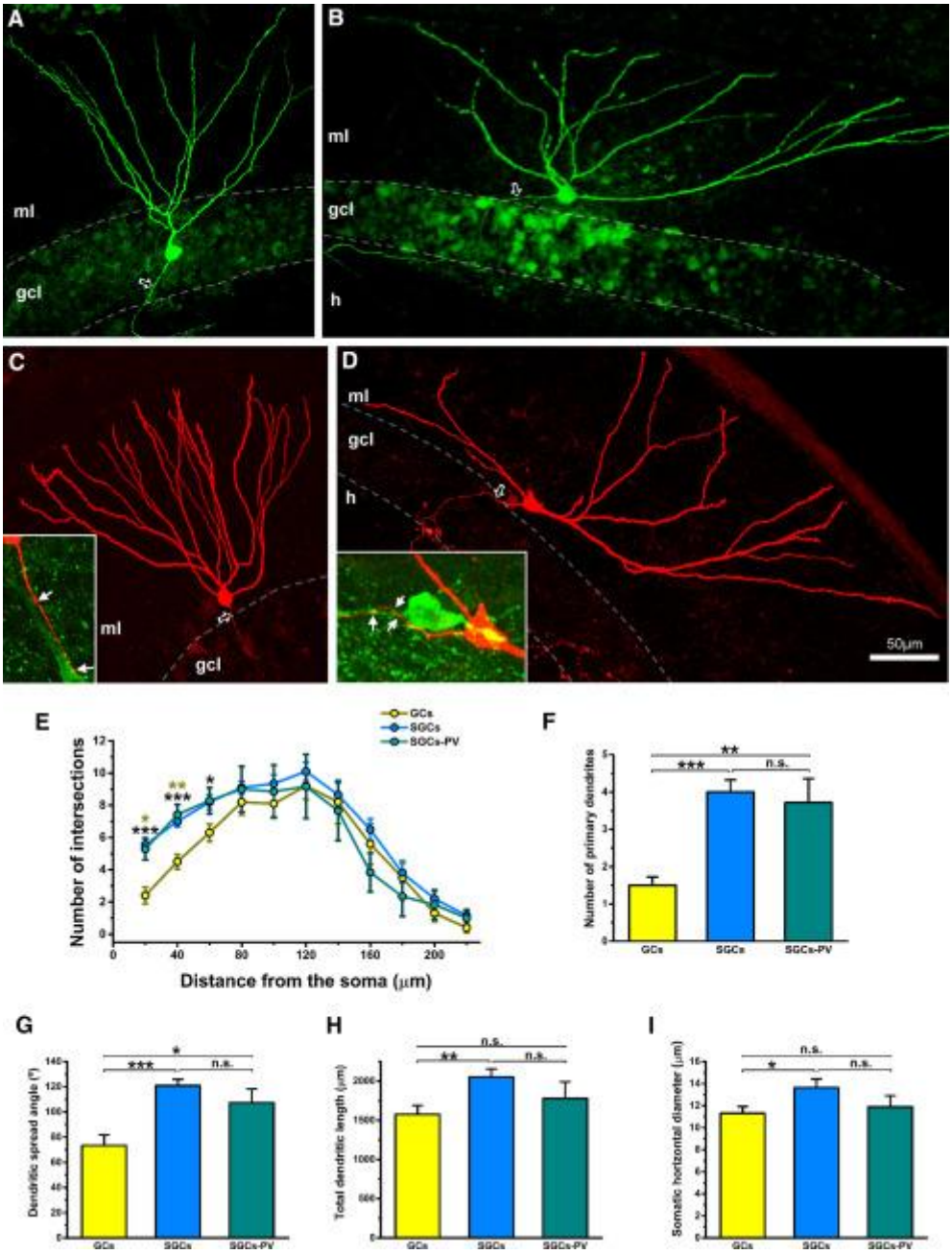


***Figure 5. The morphology of SGCs differs from GCs.*** *A, Example of a GC. One dendrite arises from the soma, the axon arises vertically and goes directly toward the hilus (arrow).* ***B****, Example of a SGC. In contrast to the GCs, several dendrites arise from the soma and the dendritic tree spans wider. The axon arises horizontally and enters the granule cell layer after running in the inner molecular layer (arrow).* ***C****,* ***D****, Two examples of SGCs. Their axons (open arrowhead) travel closely to PV-IRs. Insets show some of the biocytin-filled boutons (arrows) in close apposition to parvalbumin+ profiles.* ***E–I****,*

*Morphological analysis revealed that GCs and SGCs differed from each other in a number of morphological features. Those SGCs that formed close contacts with PV-IRs (SGC-PV) could not be distinguished from SGCs. Compared to GCs SGCs and SGC-PVs differed in the number of intersections close to their somata (E), formed more primary dendrites (F), had a larger dendritic spread angle. SGCs, but not SGC-PVs, also had a larger total dendritic length and somatic horizontal diameter (H, I). Black symbols label differences between GCs and SGCs, khaki symbols label significance between GCs and SGCs innervating parvalbumin INs. Asterisks show significance of the statistical analysis; *p < 0.05, **p < 0.01, ***p < 0.001; Abbreviations: gcl, granule cell layer; h, hilus; iml, inner molecular layer; ml, molecular layer; n.s., not significant, SGC-PV, SGC forming close contact with PV-IRs. Scale bar: 50 µm. Source:* [105]

Finally, to verify that the close contacts formed by the axons of SGCs on the PV-IRs are synapses we have inspected the close contacts with correlated light- and electron microscopy. We performed these experiments on slices in which the SGC axon formed juxtapositioned contact with PV-IRs, the ultrastructure was well preserved and the penetration of the parvalbumin antibodies were acceptable. By reconstructing the axonal segments close to the PV-IRs we found that they form asymmetric synapses to the perisomatic region of PV-IRs **(Fig. 6)**. The morphology of the biocytin-filled boutons was small and filled with round vesicles resembling to the Timm-positive boutons described previously [59] **(Fig. 6B)**. Taken together, our results show that in the DG SGCs give rise – at least partially – to the perisomatic asymmetric synapses on the PV-IRs [105].

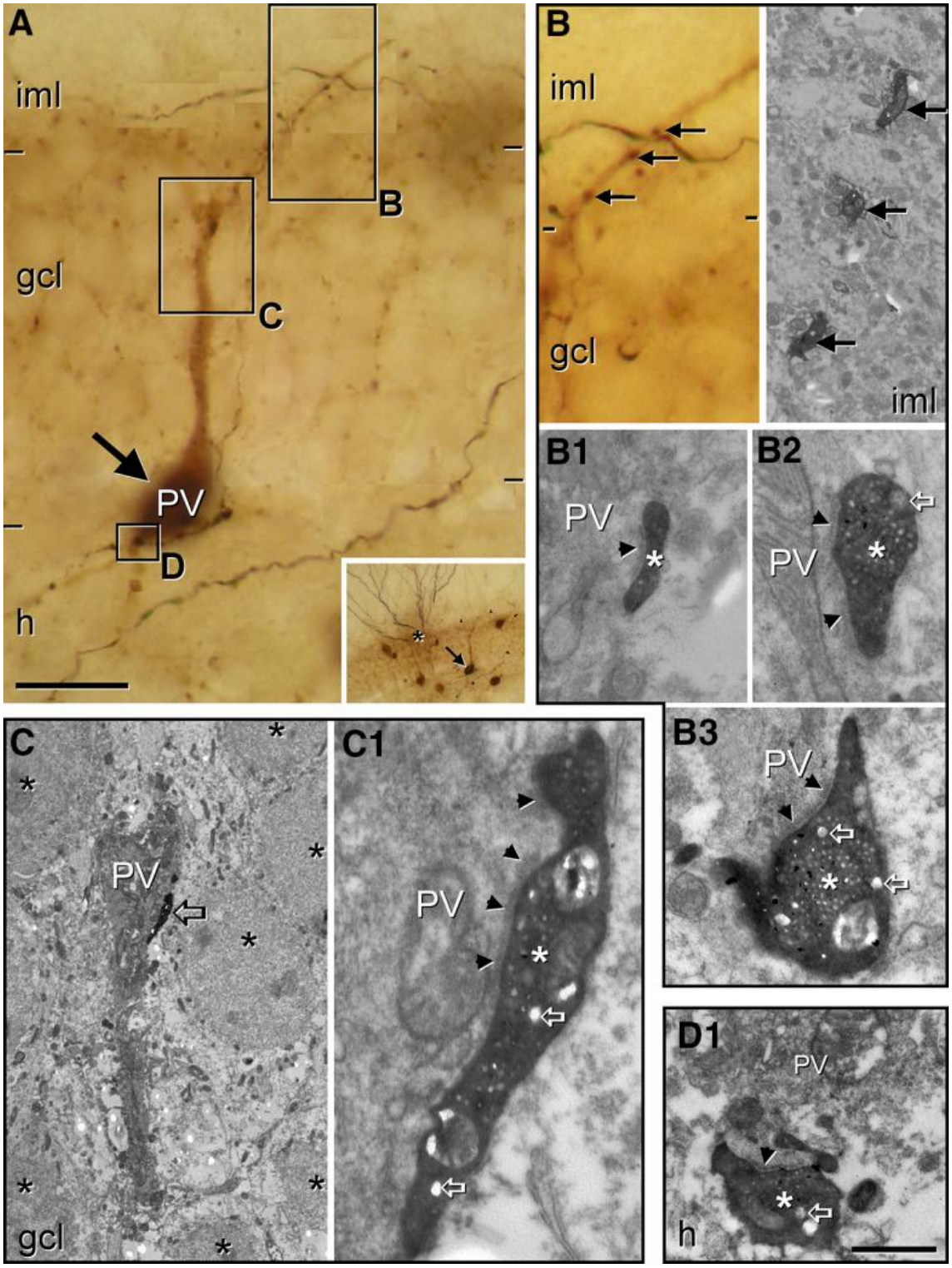


***Figure 6. Axons of SGCs form asymmetric synapses on the perisomatic region of parvalbumin cells located in the granule cell layer.*** *A SGC was filled with biocytin using patch-clamp technique. The slice was fixed and immunostaining against parvalbumin has been done. Biocytin was developed with DAB-Ni, while parvalbumin was labeled with*

*DAB. Correlated light – and electron microscopy was performed to determine if the close contacts the SGC form on the PV+ cell are synaptic contacts.* ***A****, An axon from this SGC (black) running in the inner molecular layer (arrowheads) sends a collateral toward the hilus delineating a parvalbumin cell labelled with DAB (brown). In the inset, the relative position of the SGC in the inner molecular layer (asterisk) and the parvalbumin cell (arrow) is shown. The boxes show axonal varicosities of the SGC opposing the distinct portions of the parvalbumin cell in the inner molecular layer (****B****) the granule cell layer (****C****) and the hilus (****D****).* ***B****, SGC axon giving rise to varicosities (arrows) along a thin parvalbumin dendrite originating from the parvalbumin cell in the inner molecular layer (left panel). The same string of boutons is presented on an electron micrograph shown in the right panel.* ***B1–B3****, Higher magnification of boutons shown in* ***B*** *at the level where they form large asymmetric synapses on the parvalbumin dendrite (arrowheads). The boutons are filled with round vesicles as well as many dense core vesicles (open arrows).* ***C****, A correlative electron microscopic image taken from the granule cell layer (asterisks label granule cells) shown in* ***A****. A large bouton from the SGC (open arrow) contacting the parvalbumin cell.* ***C1****, This large bouton (asterisk) makes an asymmetric synapse (arrowheads) on the parvalbumin cell and is filled with round vesicles and dense core vesicles (open arrows).* ***D1****, Bouton (asterisk) from the SGC in the juxtagranular hilus makes asymmetric synapse on a proximal dendrite of the parvalbumin IN (arrowhead). gcl, granule cell layer; h, hilus; iml, inner molecular layer; oml, outer molecular layer. Scale bar: 20 μm (****A****) and 500 nm (****B–D****). Source:* [105]

## 4.2 RESULTS – II.

### 4.2.1 Localization of TRPC6 channels in the rat hippocampal formation

To investigate which elements of the hippocampal formation express TRPC6 channels, we have performed immunostainings using an anti-TRPC6 polyclonal antibody developed against the C-terminus loop. First, to get an overview of the TRPC6 expression we stained the slices using immunoperoxidase technique, developed the immunoreaction with DAB and evaluated the results with light microscopy **(Fig. 7A)**. In the DG we observed strong immunostaining in the hilus and in the *str. moleculare*. In the hilus, we could observe several immunopositive dendritic profiles, while in the *str. moleculare* punctuated labeling was present along the GC dendrites **(Fig. 7A, B)**.

In the hippocampus proper, there was strong immunolabeling at the border of the *str. oriens*/*alveus* and in the *str. lucidum*. Further immunoreactive profiles could be observed in the *strata radiatum* and *lacunosum-moleculare* **(Fig. 7A, C)**. In the *strata radiatum* and oriens we observed smooth, immunopositive, radially running dendrites, while at the oriens/alveus horizontally running immunolabeled dendrites were also present. In the *str. lucidum,* labeled profiles seemed to outline the dendrites of the PYRs **(Fig. 7D)**. Moreover, in all layers we could observe cell bodies resembling INs. We also found immunopositive glial profiles (**Fig. (8A**).

These results indicate that TRPC6 channels are present in the input and output regions of the dentate GCs. Additionally, they are also expressed by INs [110] .

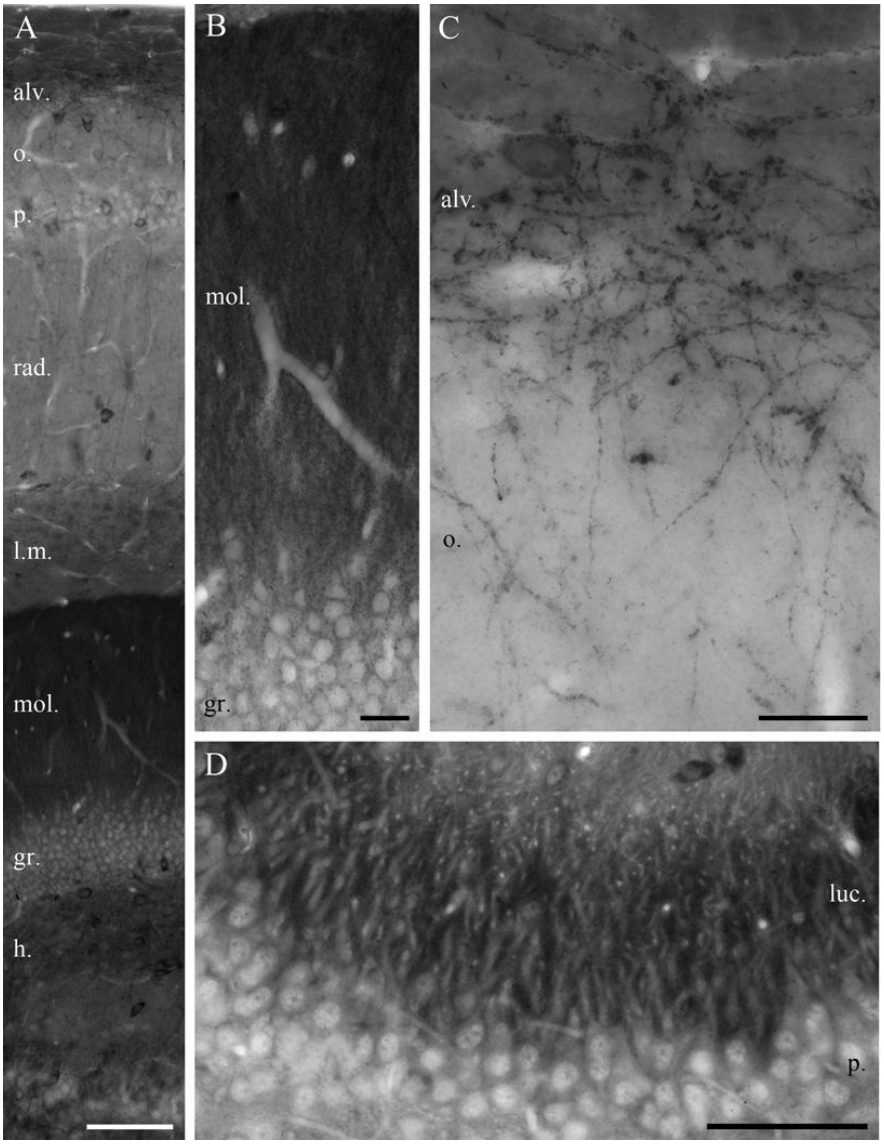


***Figure 7. Light micrographs of the rat hippocampal formation immunostained for TRPC6 protein.*** *A: Low power micrograph showing a specific laminar distribution of TRPC6-immunostaining in the CA1 region and the DG. A strong labeling can be seen in the str. moleculare of the DG in addition to numerous immunostained dendrites located both in the hilus and in strata oriens and radiatum. Moreover, some immunoreactive cell bodies resembling INs are distributed in all layers of the hippocampal formation. B: At higher magnification the dendrites of the dentate granule cells surrounded by a dense punctuated immunostaining are visible in the str. moleculare. C: In CA1, a meshwork of neuronal processes can be found at the str. oriens/alveus border formed mainly by horizontally running IN dendrites. D: In the str. lucidum of the CA3 subfield, while the main apical dendrites of CA3 PYRs appear to be immunonegative, they are outlined by a*

*dense immunostained neuropil. alv., alveus; o., stratum oriens; p., stratum pyramidale; rad., stratum radiatum; l.m., stratum lacunosum-moleculare; mol., stratum moleculare; gr., stratum granulosum; h., hilus. Scale bars: A, 100 µm; B, C, 20 µm; D, 100 µm. Source:* [110]

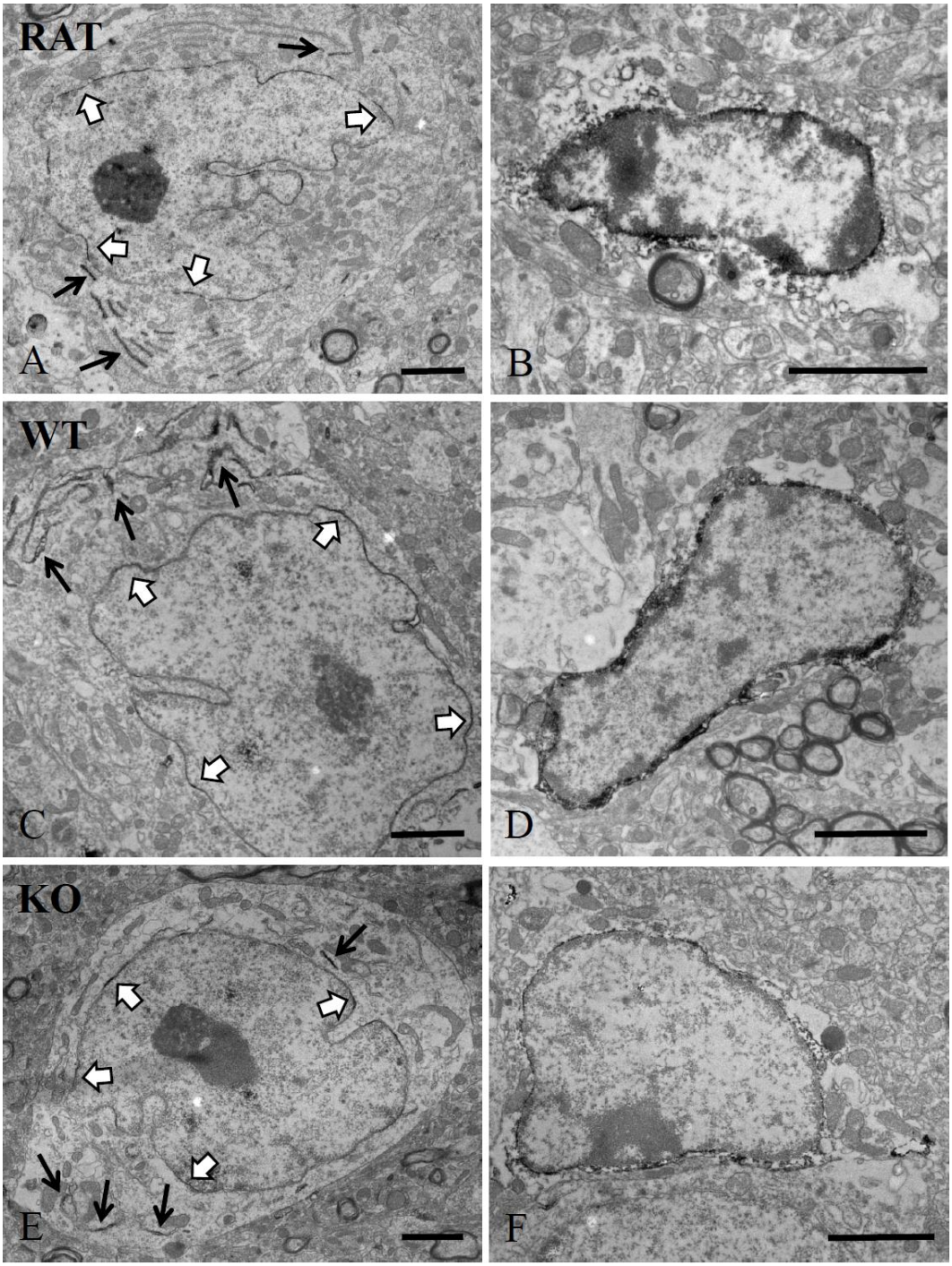

***Figure 8. In rat, wild type and Trpc6 KO mouse, the TRPC6 antibody used in this study visualizes cytoplasmic and nuclear membranes in a few INs and labels some glia cells in the same way.*** *Electron micrographs taken in rat (A), WT mouse (C) and Trpc6 KO (E) show that the immunoperoxidase reaction using DAB as a chromogen similarly labels endoplasmic reticulum (arrows) and invaginated nuclear membranes (open arrows) in some of the GABAergic cells. The invaginated membrane of the nucleus is a characteristic feature of neurons with higher metabolic rates in cortical regions, such as GABAergic neurons* [115,116]. Note, that invaginations have been also reported in the nuclei of PYRs [117] . *No labeling of the plasma membrane in the INs with cytoplasmic staining can be observed. In addition, a number of glia cells (B, D) is also stained in rat (B), WT mouse (D) and in Trpc6 KO mice (F). Scale bars, 2 µm. Source:* [110]

### 4.2.2 Localization of TRPC6 channels in the mouse hippocampal formation

Next, we aimed to validate the specificity of the antibody used in our study. To this end, we performed immunostainings on slices from Trpc6 KO mice [118]. Since our previous experiment was done on rat samples, we also repeated the immunostainings on hippocampal slices from WT mice to obtain comparable results.

In the WT mice, we observed strong immunolabeling in the str. moleculare of the dentate gyurs and a somewhat fainter labeling in the str. lucidum of the hippocampus **(Fig. 9A, C**). Immunopositive profiles resembling IN dendrites were present in the hilus, at the str. oriens/alveus border and in the strata radiatum and oriens **(Fig. 9A, B)**.

In contrast, in the Trpc6 KO mice most of the immunopositive profiles were absent both in the DG and hippocampus. The important exceptions were the cytoplasmic and glial labeling, which were present in most layers of the hippocampal formation. In light of this, we have considered the cytoplasmic and glial immunostaining aspecific and hence excluded from the further analyses (**Fig. 8, Fig. 9D, E, F**).

Taken together, these results suggest that the anti-TRPC6 antibody used in this study is specific except for cytoplasmic and glial labeling. Additionally, the immunoreactivity patterns were comparable in mice and rats [110] .

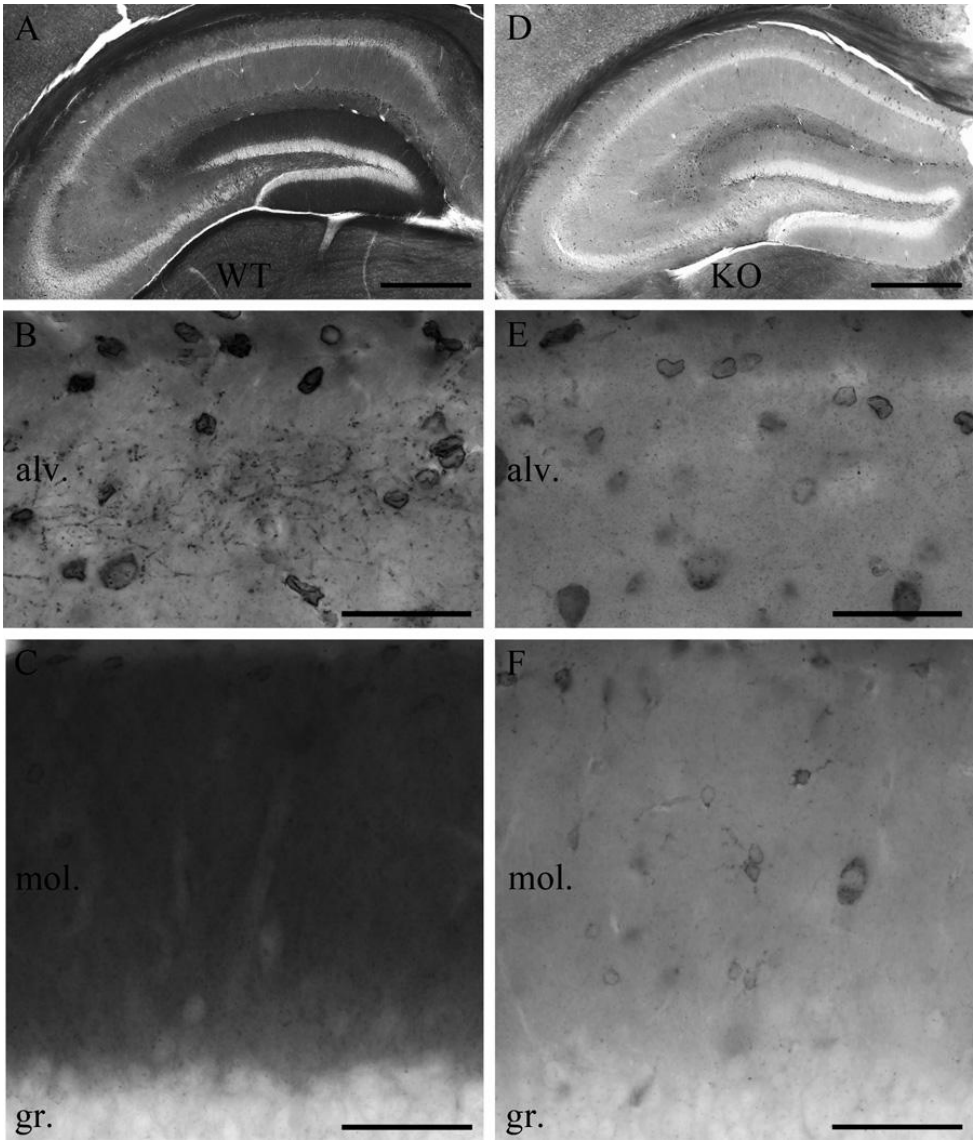


***Figure 9. Light microscopy of TRPC6 localization in the mouse hippocampal formation.*** *A: WT mice have an identical TRPC6 localization pattern to rats. An intense staining is visible in the str. moleculare of the DG. The pattern of this immunoreaction is indistinguishable from that observed in the rat DG shown at higher magnification (C). B: The meshwork of neuronal processes at the border of the str. oriens/alveus stained for TRPC6 is also present in the mouse hippocampus, comparable to that seen in the rat. D: In contrast to wild type mice, immunostaining for TRPC6 was absent in the DG in Trpc6 KO mice (F). E: Similarly, the TRPC6-immunoreactive meshwork formed mainly by interneuronal dendrites in CA1 was not visible in KO mice. However, the cell body staining with this TRPC6 antibody was comparable both in WT and Trpc6 KO mice,*

*indicating that this signal is unrelated to the presence of TRPC6 protein. Scale bars: A, D, 500 µm; B, C, E, F, 50 µm. Source:* [110]

### 4.2.3 TRPC6 channels in the *str. moleculare*

Next, we aimed to determine the subcellular distribution of TRPC6 channels in the rat DG. To this end, we used immunogold labeling and evaluated the immunostaining with electron microscopy. In the DG, the immunogold particles were predominantly associated with the plasma membranes of the GCs (**Fig. 10A**). To determine the subcellular distribution of TRPC6 channels on the GCs we calculated the density of immunoparticles in three different compartments: the dendrites, the dendritic spines and the somata. For this, we divided the number of total immunogold particles with the total membrane length of the given compartment **(**see Methods for details**)**. We found the highest density of immunogold labeling in the dendrites (0.12 ± 0.01 gold/µm, n=150), and a significantly lower density in the spines (0.04 ± 0.01 gold/µm, n = 267) and somata (0.06 ± 0.01 gold/µm, n = 20) (M-W-U test, p = 0.002 and p = 0.02, respectively). There was no significant difference between the densities observed on the spines and somata (M-W-U test, p = 0.41) **(Fig. 10B)**. These results indicate that in GCs TRPC6 channels are predominantly expressed in the dendrites [110].

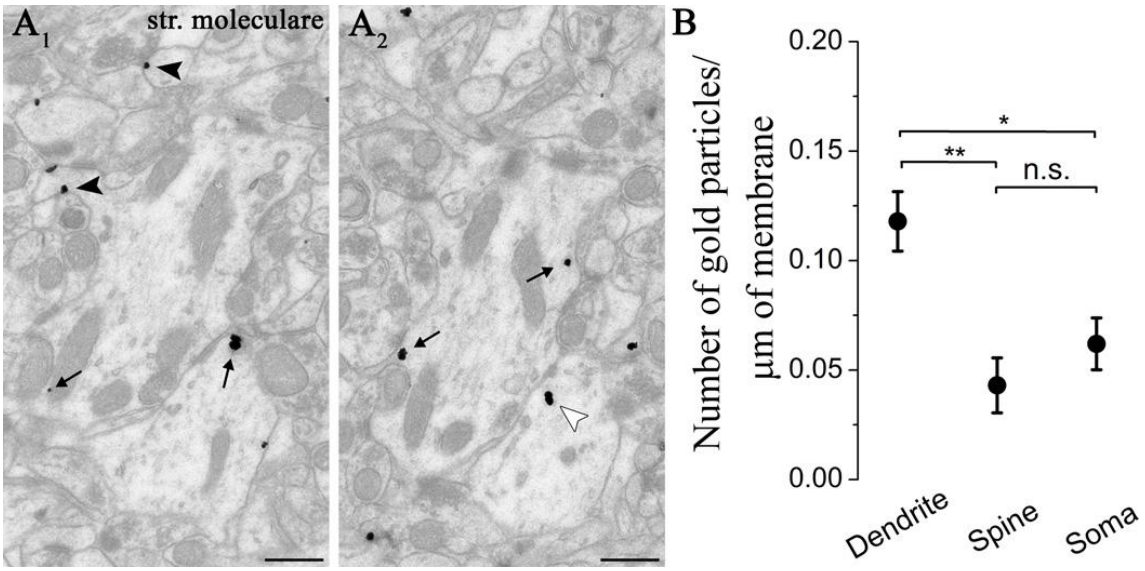

***Figure 10. TRPC6 is expressed in the plasma membrane of the dendrites, somata and spines of dentate granule cells***. *A1-2: Consecutive electron micrographs taken in the str. moleculare demonstrate that immunogold particles representing TRPC6 proteins are present on the plasma membranes of the dendrites (arrows) and spines (arrowheads) of dentate GCs. In addition, some gold particles could be occasionally seen intracellularly (open arrowhead) that may represent channels during trafficking. Scale bars: 0.5 µm. B shows the immunogold density revealed on different membrane segments. There was a significant difference in the density of immunolabeling on the surface of the dendrites and somata (marked with *, p=0.02) and dendrites and spines (marked with **, p=0.002). There was no difference in the density between spines and somata (n.s., non-significant, p=0.41). The symbols and whiskers indicate the mean and SEM, respectively. Source:* [110]

Previous results [98–100] showed that distinct membrane proteins (for example those that are involved in regulating DAG levels in spines) are localized at a given distance from the edges of excitatory synapses. With this in mind, we aimed to investigate whether TRPC6 channels are a member of this perisynaptic *annulus*. For this, we determined the sub-synaptic distribution of immunogold particles around the excitatory synapses on the dendritic spines of the GCs.

To obtain comparable results, we have followed the method of Lujan et al. [99] . We measured the distances between the immunogold particles and the closer edge of the postsynaptic densities alongside the plasma membrane on electron micrographs where both the postsynaptic density and the immunoparticles were visible **(Fig. 11A-C)**. For the analysis we sorted the values into 60 nm bins. The TRPC6 channels were evenly distributed on the surface of the dendritic spines with ~15% of the particles in the perisynaptic *annulus* around the excitatory synapses. Only very rarely (< 2%) we observed immunoparticles within the PSD or in the spine cytoplasm **(Fig. 11D)**. These results indicate that TRPC6 channels show some preference for the perisynaptic *annulus*, but most of the labeling was evenly distributed on the spines [110].

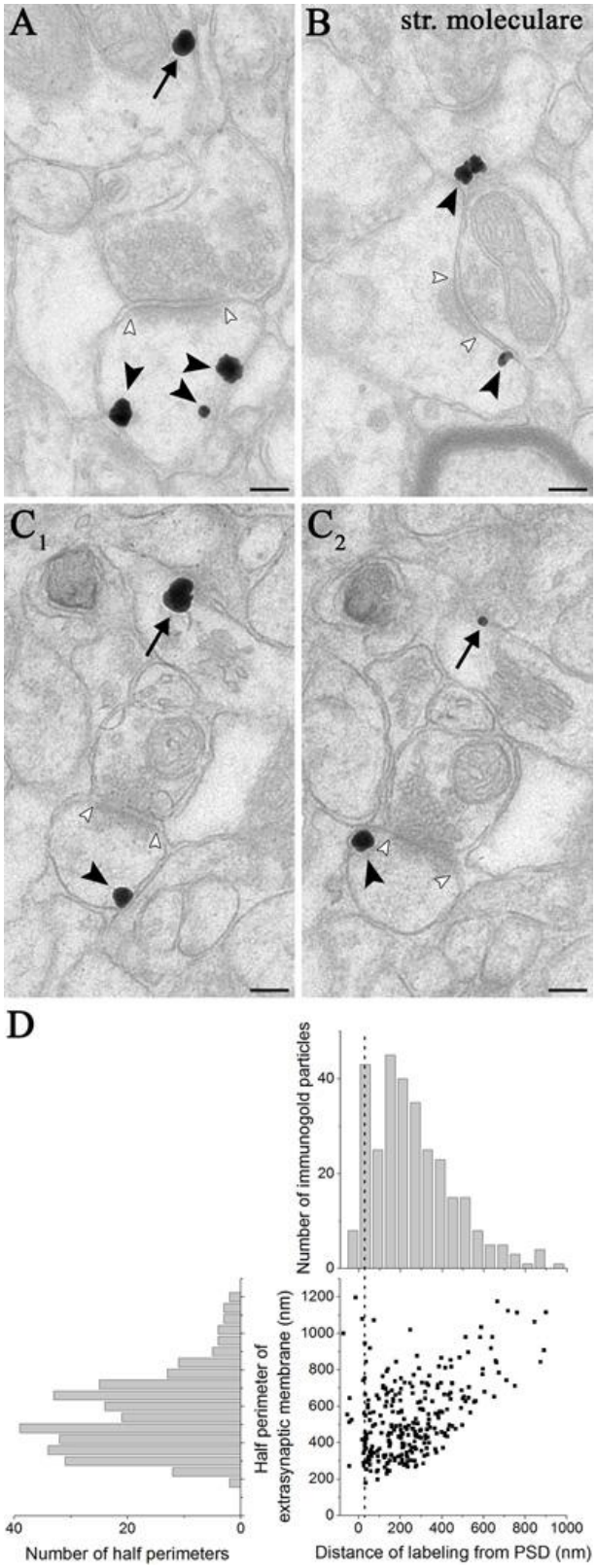
A
B
str. moleculare
C1
C2
D
Number of immunogold particles
40
20
0
Half perimeter of extrasynaptic membrane (nm)
1200
1000
800
600
400
200
0
40
20
0
Number of half perimeters
0
200
400
600
800
1000
Distance of labeling from PSD (nm)

***Figure 11. Distribution of TRPC6 on the spine heads of dentate granule cells.*** *A, B: High-resolution pre-embedding immunogold staining for TRPC6 demonstrates that this channel protein is present on the spines (arrowheads) receiving asymmetric synapses, as well as on dendrites with small diameter (arrows). C1-2: Consecutive sections of a labeled spine that receives an asymmetric synapse. Scale bars: 0.2 µm. D: Relationship between the distance of immunolabeling depicting TRPC6 and the half perimeter of extrasynaptic membrane of spines (n=279). There is a population of labeling (~ 15%), indicated with a dashed line, which is located at the edge of synapses. A larger fraction of the immunogold particles show an even distribution on the surface membrane of spines. Bar graph on top; Spatial distribution of immunogold particles in relation to the postsynaptic density (PSD) on spine heads. The distance from the edge of the synaptic junction (position 0; open arrowheads in A-C) was measured along the plasma membrane. The values were divided into 60 nm bins. Bar graph on left; Distribution of the half lengths of the perimeters of spines excluding the synaptic junction. Source:* [110]

### 4.2.4 TRPC6 channels in the *str. lucidum*

Using electron microscopy, we have investigated the subcellular distribution of the immunogold particles in the *str. lucidum*. This region is where the GC axons form the mossy terminals on CA3 PYR dendrites. We identified the mossy fibers and mossy terminals based on their characteristic morphologies. Immunogold particles were present in the axon bundles formed by the mossy fibers and in the huge boutons with multiple active zones characteristic of the mossy terminals **(Fig. 12A)**. In contrast to the dendrites and dendritic spines where the immunogold labeling were associated with the plasma membranes, in the GC axons the immunogold labeling were often localized intracellularly **(Fig. 12A)**. Additionally, in the mossy terminals immunoparticles avoided the vesicular clusters and were often associated with intracellular membrane *cisternae* or the plasma membrane **(Fig. 12B-D)**. These results indicate that in contrast to the dendrites and spines, in the axons and axon terminals of the GCs the TRPC6 channels are often expressed intracellularly. In the mossy terminals the TRPC6 channels were often expressed on intracellular membrane *cisternae* [110].

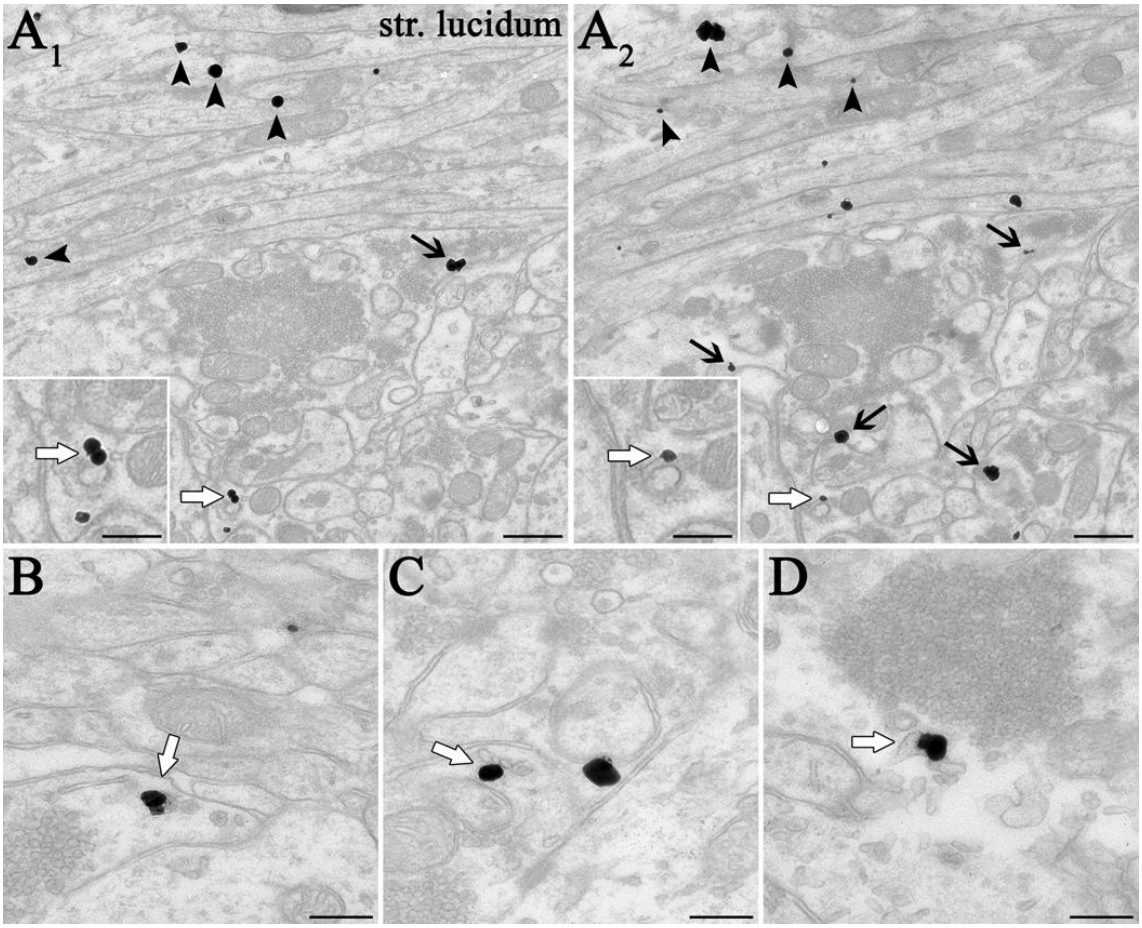


***Figure 12. TRPC6 channels are often localized intracellularly in the axons of dentate granule cells.*** *A1-2: Gold particles representing TRPC6 channels were mainly found in the en passant axons, frequently forming bundles in the str. lucidum (arrowheads). In the mossy terminals, gold labeling avoiding vesicular clusters was commonly attached to the plasma membrane or intracellular membrane cisternae (arrows). Inserts show the same structure taken from the bottom left parts of the consecutive sections, highlighting a gold particle attached to an intracellular membrane cisterna. B, C, D: High-power electron micrographs demonstrating immunogold staining associated with membrane cisternae (open arrows). Scale bars: A, 0.5 µm; insert 0.25 µm; B-D 0.2 µm. Source:* [110]

### 4.2.5 TRPC6 in the interneurons

Next, we investigated the TRPC6 distribution at the border of *str. oriens/alveus*, the *str. radiatum* and in the hilus. The immunolabeled dendritic profiles in the hilus and at the

border of the *str. oriens/alveus* resembled the dendrites of the mGluR1a-expressing [36] INs (**Fig. 7C**). We confirmed this observation with double immunostainings. We found that the vast majority of these dendrites at the border of *str. oriens/alveus* and in the hilus indeed co-express mGluR1a and TRPC6 **(Fig. 13A-F)**.

We also aimed to determine the identity of the INs with TRPC6 expressing dendrites in the *str. radiatum*. Since these radially running, smooth immunopositive dendrites resembled the dendrites of perisomatic region-targeting INs we performed double immunostainings against parvalbumin and TRPC6 [6,35] . This experiment revealed that the majority of TRPC6 dendrites in the *str. radiatum* also expressed parvalbumin **(Fig. 13G-I)**.

Together, these results show that TRPC6 are expressed by two large INs populations in the hippocampus characterized by their mGluR1a or parvalbumin content.

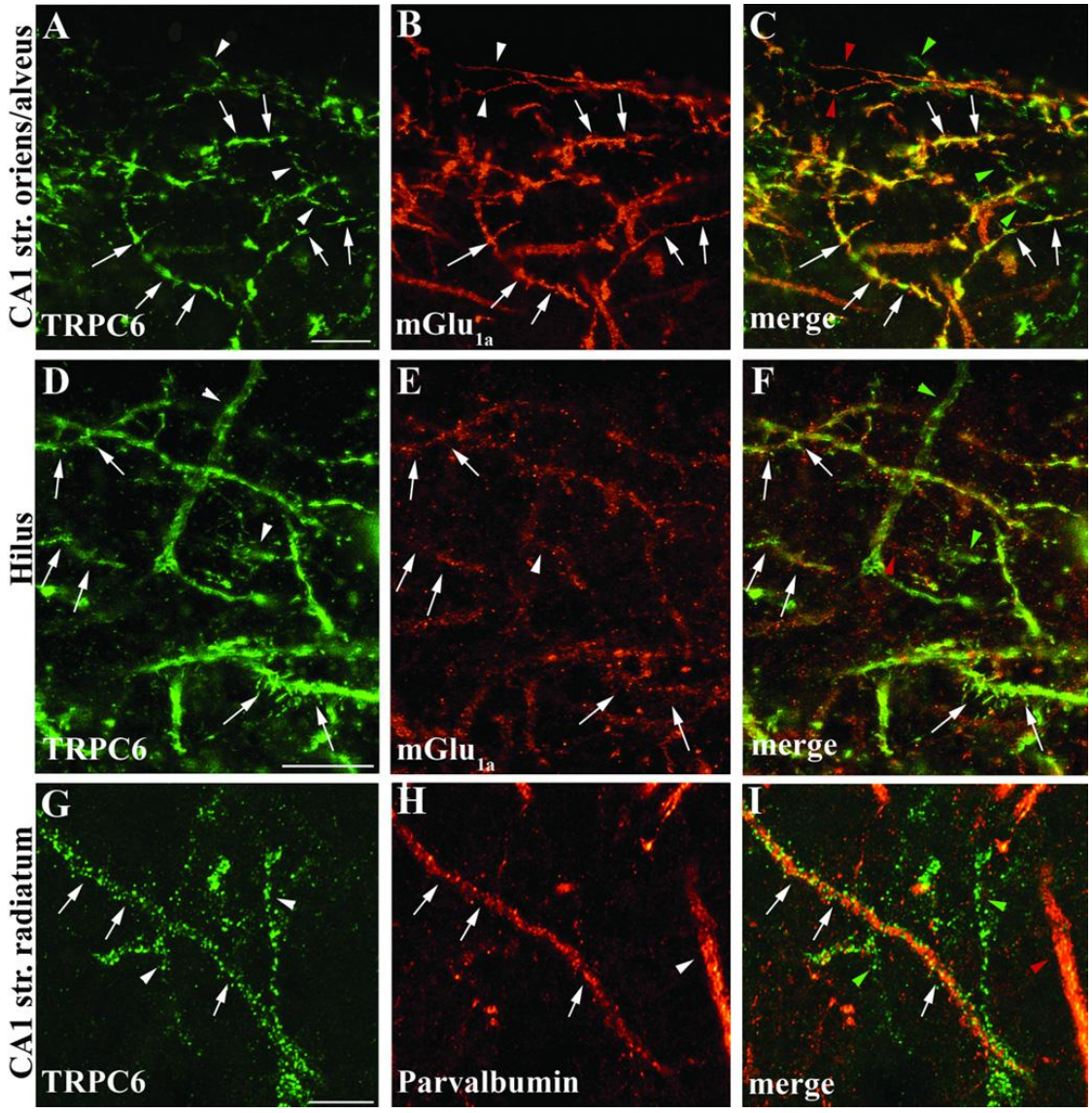


***Figure 13. TRPC6 channels are expressed by mGluR1a- or parvalbumin-immunoreactive INs in the hippocampus.*** *Double immunofluorescent staining indicates that both at the border of alveus and str. oriens, as well as in the hilus, the majority of mGluR1a -immunoreactive dendrites also express TRPC6 (white arrows). In the str. radiatum, some parvalbumin-containing dendrites are also immunoreactive for TRPC6 (white arrows). Arrowheads show singly-immunoreactive profiles, color-coded in the merged pictures. Scale bars: A, D, 10 µm; G, 5 µm. Source:*[110]

Finally, we set out to determine the subcellular distribution of TRPC6 on the IN dendrites. For this, we identified IN dendrites based on their morphologies on electron micrographs. In the hilus and *str. oriens* spiny dendrites that received asymmetric synapses on their

shafts had immunogold particles associated with their plasma membranes [17,119,120] **(Fig. 14A-B)**. These dendrites are likely to belong to mGluR1a-expressing INs. Likewise, in the *str. radiatum* the immunoparticles were also associated to the outer membrane of aspiny dendrites covered by asymmetric synapses **(Fig. 14C)**. These dendrites resemble the PV-IR dendrites [43] .

Together our results show that TRPC6 channels are associated to the plasma membrane of IN dendrites in the *hilus* and *strata oriens* and *radiatum* [110].

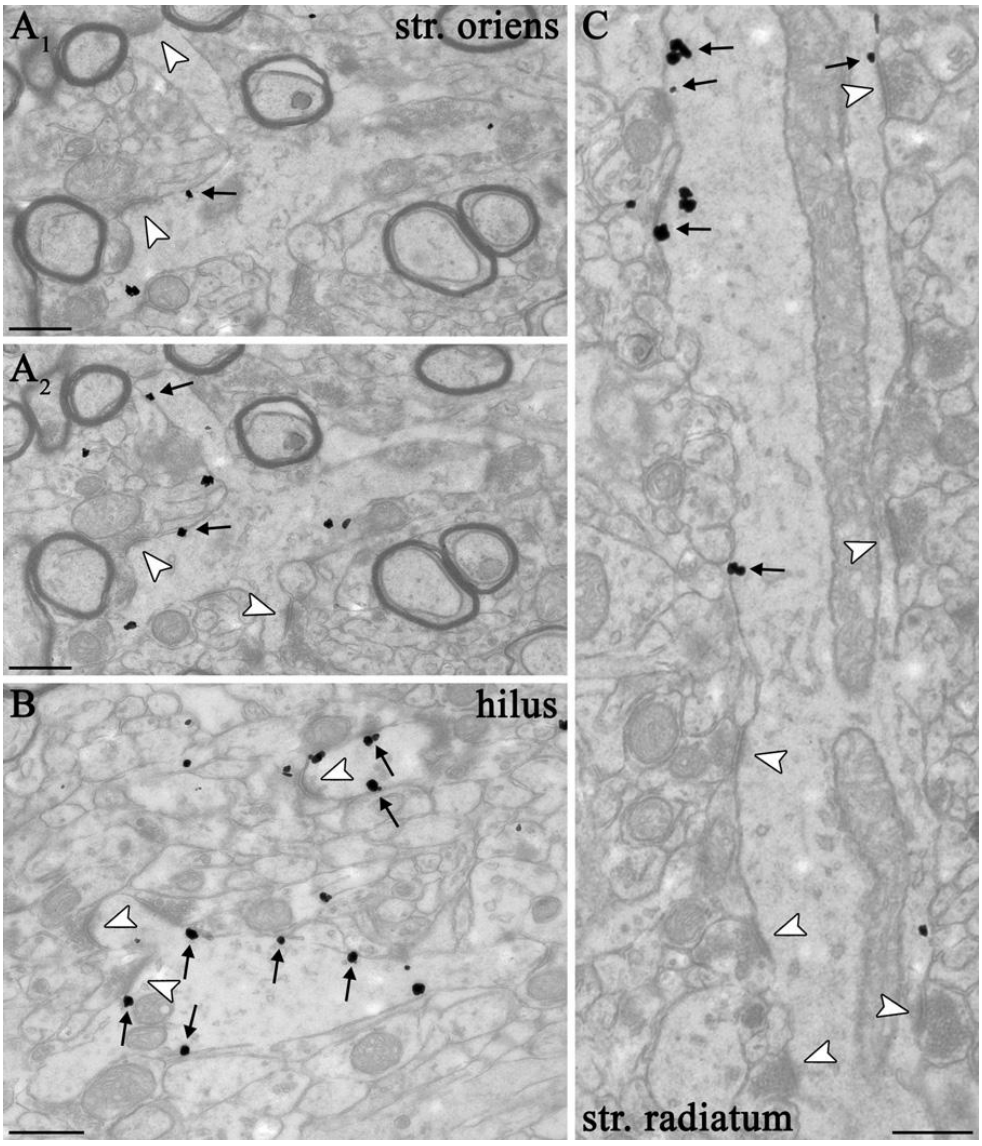


***Figure 14. Plasma membranes of IN dendrites are decorated with immunogold staining representing TRPC6 channels.*** *A1-2. Consecutive images taken in the str. oriens*

*demonstrate that TRPC6 channels depicted by gold particles (arrows) are present on the plasma membrane of horizontal IN dendrites bearing long spines and receiving asymmetric synapses on their shafts and spines (open arrowheads). B: IN dendrites in the hilus receiving asymmetric synapses on their shafts and spines (open arrowheads) are decorated with immunogold labeling. C: On the plasma membrane of an IN dendrite in the str. radiatum densely covered by asymmetric synapses (open arrowheads), which is a hallmark of PV-IRs, gold particles are attached to the intracellular surface of the plasma membrane (arrows). Scale bars: 0.5 µm. Source:* [110]

# 5. DISCUSSION

In summary, the studies presented in this thesis aimed 1) to determine the source of the perisomatic excitation on PV-IRs in the DG and 2) to reveal the cellular and subcellular distribution of TRPC6 channels in the hippocampus.

## 5.1 Semilunar granule cells form asymmetric synapses on the perisomatic region of parvalbumin-immunoreactive interneurons in the dentate gyrus

One of our goals was to uncover the source of the perisomatic excitatory inputs to the PV-IRs in the DG. Previous results showed that $Zn^{2+}$-containing, Timm-positive terminals form asymmetric synapses on the perisomatic region of PV-IRs [59,114,121,122] . However, it was presumed that GCs give rise to these inputs as the high $Zn^{2+}$-levels and the ultrastructural features resembled to the terminals of the GCs [7,17,59] .

In contrast to this hypothesis, our light- and electron microscopic data shows that a distinct excitatory cell type of the DG, the SGCs give rise to the perisomatic excitation of the PV-IRs in the DG. In our dataset, we identified morphological differences between GCs and SGCs and found the SGC axons contact the perisomatic region of PV-IRs. Our subsequent electron microscopic analysis of these close contacts confirmed that SGCs form asymmetric synapses on the PV-IRs. The morphology of these boutons was strikingly similar to the previously reported Timm-positive boutons contacting the perisomatic region of PV-IRs. Taken together, our results underline that the asymmetric synapses are partially if not fully are formed by SGCs on the perisomatic region of PV-IRs in the mouse DG.

Several studies are pointing to the significance of SGCs [78,82,123]. The circuit motif of perisomatic excitation on the perisomatic region of PV-IRs is a characteristic shown in other cortical regions as well [55–58] . Based on our results in the DG the SGCs fulfill this function. Thus, these neurons could have a profound effect of the DG circuitry through activating a strong feed-forward inhibition. Moreover, SGCs have been shown to reciprocally innervate MCs. It has been also shown that during hilar UP-states MCs and SGCs are active together [82].

This special position of SGCs suggests their critical role in several DG functions. The DG circuitry performs pattern separation, and a prerequisite of this function is the sparse firing of the dentate GCs. SGCs could contribute to the sparse activation of GCs through the activation of fast-spiking INs in a feed-forward manner. This is further underlined by results showing, that PV-IRs exhibit highly abundant lateral inhibition in the DG [124] Meanwhile SGCs could also participate in excitation of the GC dendrites through the activation of MCs. Additionally, SGCs have been shown to receive a lower activity-dependent increase of feed-back inhibition during afferent activation that could facilitate their increased firing upon perforant path stimulation [80]. Thus, a handful of GCs that receive excitation both from MCs (and indirectly from SGCs) and the perforant path would overcome the perisomatic inhibition dictated by PV-IRs [66,70,105,125,126].

SGCs are overrepresented in experiments using FosTRAP and FosTRAP2 reporter mice to label active neurons during hippocampal-related behaviors such as contextual memory formation or exploration in novel environments. These important new results highlight the potential behavioral relevance of SGCs, however further research will be required as physiological properties of SGCs themselves could explain their overrepresentation in c-Fos labeled neuronal populations [77,81].

## 5.2 Distribution of TRPC6 channels in the hippocampus

Our results show that TRPC6 channels are expressed in all compartments of the GCs: somata, dendrites, dendritic spines, axons and axon terminals. In the dendrites, spines and somata the TRPC6 channels are located in the plasma membranes. On the dendritic spines the TRPC6 channels are somewhat enriched in a perisomatic *annulus* around the synapse but are evenly distributed otherwise. In contrast, in the axons of GCs, the TRPC6 channels are frequently located intracellularly, however, in the axon terminals they are often associated with membrane *cisternae* while eluding the vesicular clusters. Moreover, we found that both mGluR1a-expressing and PV-IR populations express TRPC6 channels in the plasma membranes of their dendrites.

### 5.2.1 TRPC6 in dentate granule cells

Using immunogold labeling, we determined the subcellular distribution of TRPC6 channels in the GC dendritic spines. As DAG directly activates TRPC6 channels [88,127] therefore we aimed to compare its subcellular distribution on spines to proteins regulating DAG levels.

Such proteins, for example mGluR5, PLCβ1/4 and DAG lipase, are present around excitatory synapses as members of a perisynaptic *annulus* [99–103,128]. As at least a part of the TRPC6 channels are also members of this *annulus,* it suggests that TRPC6 channels may play a role in related signalization pathways. For example, mGluR5-dependent depolarization and the subsequent $Ca^{2+}$ influx might be partially mediated by TRPC6 channels. Increased $Ca^{2+}$-level has been also proposed as a feedback signal for closure of mGluR5 channels, thus TRPC6 channels could serve as part of a negative feedback signalization [88,97] . In turn, $Ca^{2+}$ influx also increases the activity of DAG lipase, which degrades DAG that activates TRPC6 channels. Therefore, the mGluR5-dependent PLCβ activation could also regulate the closure of TRPC6 channels. Although some of these results have been shown in hippocampal neurons, all these molecular components are present in the dentate GCs, as well [98,129,130].

In GCs TRPC6 channels are also present in the plasma membranes of dendritic shafts and cell bodies. Importantly, all the above-mentioned signalization components are present in these compartments. Thus, a similar mechanism of TRPC6 channel regulation could take place here [99,119,131] . Additionally, all metabotropic receptors using the $G_q$ protein-mediated signalization pathways, such as the mGluR1, TrkB or type1 muscarinic receptors, could activate TRPC6 channels. Previously it has been shown that these G protein-coupled receptors can be found on the spines of PCs where they may open DAG-sensitive TRPC channels mediating cation influx into the spines of cortical excitatory cells.

In the mossy fibers we often found TRPC6 channels intracellularly, while in the mossy terminals they were associated with intracellular membrane *cisternae*. This suggests that TRPC6 channels may also play a role in calcium-induced calcium release (CICR). During CIRC increased intracellular $Ca^{2+}$-levels lead to $Ca^{2+}$-release from intracellular stores [90,132,133] . This has been proposed as a mechanism through which $Ca^{2+}$-signals can

be amplified in the mossy terminals in an activity-dependent manner [134] . It has been previously demonstrated by Shimizu et al. that RyR2 are present in mossy fibers and mossy terminals where they are involved in CICR. RyR2 also avoided the active zones and were associated with membrane *cisternae* resembling smooth ERs. This pattern is strikingly similar to the localization of TRPC6 channels reveled by our study. Therefore, we hypothesize that TRPC6 channels and RyR2 are together involved in mediating CIRC in dentate GC axons and terminals. Thus, this also suggests that TRPC6 channels could be involved in presynaptic plasticity mechanisms in the mossy terminals [134] .

As TRPC6 channels are present in all major compartments of the dentate GCs: somata, dendrites, dendritic spines, axons and mossy terminals, we propose that these channels are in a crucial position to mediate information flow at the first step of the hippocampal circuitry [110].

### 5.2.2 TRPC6 in hippocampal interneurons

We have revealed the presence of TRPC6 channels in the dendrites of both mGluR1a-expressing and PV-expressing IN populations. As mGluR1a or mGluR5, TrkB and DAG lipase are all expressed in these INs, it is possible that TRPC6 channels are similarly regulated here as in the dentate GCs [99,119,135,136] . Moreover, in INs it has been shown that $Ca^{2+}$ entering through TRP-like channels can play a role in plasticity mechanisms [136] . Importantly, mGluR1a and PV are markers of two major groups of INs in the hippocampus: the feed-forward and feed-back INs. Thus, TRPC6 channels could be also involved in regulating both types of inhibition in the hippocampal circuitry [137] .

Altogether, our results show that TRPC6 channels are expressed by key players of hippocampal neural networks highlighting the fundamental roles they might play in the hippocampal function [110].

## 6. CONCLUSIONS

In our studies presented in this PhD dissertation we have 1) revealed the source of the perisomatic excitatory synapses on PV-IRs in the mouse DG and 2) determined the cellular and subcellular distribution of TRPC6 channels in the rat hippocampus.

The results presented in the first part of this thesis show that in the DG SGCs give rise to the perisomatic excitatory synapses on PV-IRs. Thus, this sparse PC type is in an influential position within the DG network, likely contributing to pattern separation by activating feed-forward inhibition.

Our results presented in the second part of the dissertation show that in the hippocampus the DAG-sensitive, $Ca^{2+}$-permeable TRPC6 channels are expressed by the dentate GCs and two functionally distinct populations of INs.

In the dendrites, dendritic spines and cell bodies of the GCs the TRPC6 channels are expressed in the plasma membranes. In the spines the TRPC6 channels are evenly distributed showing an enrichment at the edge of the postsynaptic densities, where these channels overlap with proteins involved in the regulation of DAG levels. In the mossy fibers TRPC6 channels are localized intracellularly, whereas these channels are often associated to membrane *cisternae* in the axon terminals. In the axons and axon terminals TRPC6 localization is similar to that revealed for RyR2 suggesting that TRPC6 channels may be involved in controlling calcium-induced $Ca^{2+}$ - release and presynaptic plasticity.

We also show that in the hippocampus TRPC6 channels are expressed in the dendrites of two IN populations, characterized by their mGluR1a and parvalbumin expression. These IN populations have been suggested to fulfil feed-forward and feed-back inhibition, respectively.

Taken together our results show that TRPC6 channels are in position to participate hippocampal information processing through regulating the input and output of GCs and through modulating feed-forward and feedback inhibition [110].

## 7. SUMMARY

The hippocampus plays a fundamental role in several physiological functions such as memory and spatial navigation and pathological conditions such as depression or epilepsy. Despite decades of intensive research, several details of the hippocampal operation are still not known. The DG, a part of the hippocampus, is a brain region known to be critical in processing the multimodal information transmitted from cortical regions to the hippocampus. One type of inhibitory cells, PV-IRs, play a key role in DG functions. These INs receive excitatory inputs on their perisomatic region; however, the source of these synapses has been unknown. In the work presented in the first part of my thesis we used a combination of immunohistochemistry, light and electron microscopy, and *in vitro* patch clamp electrophysiology to address this question. Our results indicate that in the DG, SGCs are the primary source of perisomatic excitatory synapses on PV-IRs.

TRPC6 channels are DAG-sensitive, $Ca^{2+}$-permeable, non-selective cation channels. These channels are selectively activated by hyperforin, the active constituent of Hypericum perforatum (St John's wort). Hyperforin has mild antidepressant effects and has a neuroprotective effect during seizures. TRPC6 channels have also been proposed to be involved in the formation and maintenance of excitatory synapses and dendritic spines. To understand how TRPC6 channels are involved in hippocampal functions, in our work presented in the second part of my thesis, we aimed to determine its cellular and subcellular distribution in the hippocampus using immunohistochemistry and light and electron microscopy. Our results show that TRPC6 channels are expressed in the dendrites, spines, somata, axons and axon terminals of the GCs. In the dendrites, spines and cell bodies of the GCs, the TRPC6 channels are expressed in the plasma membranes. In the spines, the TRPC6 channels are evenly distributed showing an enrichment at the edge of the synapses. In the axons and terminals TRPC6 channels are frequently localized intracellularly, in the terminals often associated to membrane *cisternae*. We also show that in the hippocampus, TRPC6 channels are expressed in the dendrites of two interneuron populations expressing mGluR1a or parvalbumin.

Taken together, these results lead to a better understanding of the possible roles of SGCs and TRPC6 channels in the hippocampus and open the way for further, functional investigations.

8. REFERENCES


1. Buzsáki G, Moser EI. Memory, navigation and theta rhythm in the hippocampal-entorhinal system. Nat Neurosci. 2013;16(2):130–8. doi:10.1038/nn.3304 PubMed PMID: 23354386; PubMed Central PMCID: PMC4079500.

2. Eichenbaum H. Hippocampus Cognitive Processes and Neural Representations that Underlie Declarative Memory. Neuron. 2004;44(1):109–20. doi:10.1016/j.neuron.2004.08.028 PubMed PMID: 15450164.

3. Squire LR, Stark CEL, Clark RE. THE MEDIAL TEMPORAL LOBE*. Annu Rev Neurosci. 2004;27(1):279–306. doi:10.1146/annurev.neuro.27.070203.144130 PubMed PMID: 15217334.

4. Scoville WB, Milner B. LOSS OF RECENT MEMORY AFTER BILATERAL HIPPOCAMPAL LESIONS. J Neurol, Neurosurg Psychiatry. 1957;20(1):11. doi:10.1136/jnnp.20.1.11 PubMed PMID: 13406589; PubMed Central PMCID: PMC497229.

5. Amaral DG, Witter MP. The three-dimensional organization of the hippocampal formation: A review of anatomical data. Neuroscience. 1989;31(3):571–91. doi:10.1016/0306-4522(89)90424-7 PubMed PMID: 2687721.

6. Freund TF, Buzsáki G. Interneurons of the hippocampus. Hippocampus. 1996;6(4):347–470. doi:10.1002/(sici)1098-1063(1996)6:4<347::aid-hipo1>3.0.co;2-i PubMed PMID: 8915675.

7. Claiborne BJ, Amaral DG, Cowan WM. Quantitative, three-dimensional analysis of granule cell dendrites in the rat dentate gyrus. J Comp Neurol. 1990;302(2):206–19. doi:10.1002/cne.903020203 PubMed PMID: 2289972.

8. Strien NM van, Cappaert NLM, Witter MP. The anatomy of memory: an interactive overview of the parahippocampal–hippocampal network. Nat Rev Neurosci. 2009;10(4):272–82. doi:10.1038/nrn2614 PubMed PMID: 19300446.

9. Basu J, Siegelbaum SA. The Corticohippocampal Circuit, Synaptic Plasticity, and Memory. Cold Spring Harb Perspect Biol. 2015;7(11):a021733. doi:10.1101/cshperspect.a021733 PubMed PMID: 26525152; PubMed Central PMCID: PMC4632668.

10. Knierim JJ, Neunuebel JP. Tracking the flow of hippocampal computation: Pattern separation, pattern completion, and attractor dynamics. Neurobiol Learn Mem. 2016;129:38–49. doi:10.1016/j.nlm.2015.10.008 PubMed PMID: 26514299; PubMed Central PMCID: PMC4792674.

11. Cayco-Gajic NA, Silver RA. Re-evaluating Circuit Mechanisms Underlying Pattern Separation. Neuron. 2019;101(4):584–602. doi:10.1016/j.neuron.2019.01.044 PubMed PMID: 30790539; PubMed Central PMCID: PMC7028396.

12. Yassa MA, Stark CEL. Pattern separation in the hippocampus. Trends Neurosci. 2011;34(10):515–25. doi:10.1016/j.tins.2011.06.006 PubMed PMID: 21788086; PubMed Central PMCID: PMC3183227.

13. Guzman SJ, Schlögl A, Espinoza C, Zhang X, Suter BA, Jonas P. How connectivity rules and synaptic properties shape the efficacy of pattern separation in the entorhinal cortex–dentate gyrus–CA3 network. Nat Comput Sci. 2021;1(12):830–42. doi:10.1038/s43588-021-00157-1 PubMed PMID: 38217181.

14. Witter MP. The perforant path: projections from the entorhinal cortex to the dentate gyrus. Prog Brain Res. 2007;163:43–61. doi:10.1016/s0079-6123(07)63003-9 PubMed PMID: 17765711.

15. Schmidt B, Marrone DF, Markus EJ. Disambiguating the similar: The dentate gyrus and pattern separation. Behav Brain Res. 2012;226(1):56–65. doi:10.1016/j.bbr.2011.08.039 PubMed PMID: 21907247.

16. Amaral DG, Ishizuka N, Claiborne B. Chapter 1 Chapter Neurons, numbers and the hippocampal network. Prog Brain Res. 1990;83:1–11. doi:10.1016/s0079-6123(08)61237-6 PubMed PMID: 2203093.

17. Acsády L, Kamondi A, Sík A, Freund T, Buzsáki G. GABAergic Cells Are the Major Postsynaptic Targets of Mossy Fibers in the Rat Hippocampus. J Neurosci. 1998;18(9):3386–403. doi:10.1523/jneurosci.18-09-03386.1998 PubMed PMID: 9547246.

18. Acsády L, Káli S. Models, structure, function: the transformation of cortical signals in the dentate gyrus. Prog Brain Res. 2007;163:577–99. doi:10.1016/s0079-6123(07)63031-3 PubMed PMID: 17765739.

19. Henze DA, Urban NN, Barrionuevo G. The multifarious hippocampal mossy fiber pathway: a review. Neuroscience. 2000;98(3):407–27. doi:10.1016/s0306-4522(00)00146-9 PubMed PMID: 10869836.

20. Claiborne BJ, Amaral DG, Cowan WM. A light and electron microscopic analysis of the mossy fibers of the rat dentate gyrus. J Comp Neurol. 1986;246(4):435–58. doi:10.1002/cne.902460403 PubMed PMID: 3700723.

21. Lisman JE. Relating Hippocampal Circuitry to Function Recall of Memory Sequences by Reciprocal Dentate–CA3 Interactions. Neuron. 1999;22(2):233–42. doi:10.1016/s0896-6273(00)81085-5 PubMed PMID: 10069330.

22. Ito HT, Schuman EM. Functional division of hippocampal area CA1 via modulatory gating of entorhinal cortical inputs. Hippocampus. 2012;22(2):372–87.

doi:10.1002/hipo.20909 PubMed PMID: 21240920; PubMed Central PMCID: PMC3627339.

23. Brun VH, Otnæss MK, Molden S, Steffenach HA, Witter MP, Moser MB, Moser EI. Place Cells and Place Recognition Maintained by Direct Entorhinal-Hippocampal Circuitry. Science. 2002;296(5576):2243–6. doi:10.1126/science.1071089 PubMed PMID: 12077421.

24. Remondes M, Schuman EM. Role for a cortical input to hippocampal area CA1 in the consolidation of a long-term memory. Nature. 2004;431(7009):699–703. doi:10.1038/nature02965 PubMed PMID: 15470431.

25. Levy WB, Desmond NL, Zhang DX. Perforant path activation modulates the induction of long-term potentiation of the schaffer collateral--hippocampal CA1 response: theoretical and experimental analyses. Learn Mem. 1998;4(6):510–8. doi:10.1101/lm.4.6.510 PubMed PMID: 10701875.

26. Dvorak-Carbone H, Schuman EM. Long-Term Depression of Temporoammonic-CA1 Hippocampal Synaptic Transmission. J Neurophysiol. 1999;81(3):1036–44. doi:10.1152/jn.1999.81.3.1036 PubMed PMID: 10085331.

27. Dudman JT, Tsay D, Siegelbaum SA. A Role for Synaptic Inputs at Distal Dendrites: Instructive Signals for Hippocampal Long-Term Plasticity. Neuron. 2007;56(5):866–79. doi:10.1016/j.neuron.2007.10.020 PubMed PMID: 18054862; PubMed Central PMCID: PMC2179894.

28. Blaabjerg M, Zimmer J. The dentate mossy fibers: structural organization, development and plasticity. Prog Brain Res. 2007;163:85–803. doi:10.1016/s0079-6123(07)63005-2 PubMed PMID: 17765713.

29. Hangya B, Borhegyi Z, Szilágyi N, Freund TF, Varga V. GABAergic Neurons of the Medial Septum Lead the Hippocampal Network during Theta Activity. J Neurosci. 2009;29(25):8094–102. doi:10.1523/jneurosci.5665-08.2009 PubMed PMID: 19553449; PubMed Central PMCID: PMC6666051.

30. Mizuseki K, Sirota A, Pastalkova E, Buzsáki G. Theta Oscillations Provide Temporal Windows for Local Circuit Computation in the Entorhinal-Hippocampal Loop. Neuron. 2009;64(2):267–80. doi:10.1016/j.neuron.2009.08.037 PubMed PMID: 19874793; PubMed Central PMCID: PMC2771122.

31. Klausberger T, Somogyi P. Neuronal Diversity and Temporal Dynamics: The Unity of Hippocampal Circuit Operations. Science. 2008;321(5885):53–7. doi:10.1126/science.1149381 PubMed PMID: 18599766; PubMed Central PMCID: PMC4487503.

32. Tzilivaki A, Tukker JJ, Maier N, Poirazi P, Sammons RP, Schmitz D. Hippocampal GABAergic interneurons and memory. Neuron. 2023. doi:10.1016/j.neuron.2023.06.016

33. Kepecs A, Fishell G. Interneuron cell types are fit to function. Nature. 2014;505(7483):318–26. doi:10.1038/nature12983 PubMed PMID: 24429630; PubMed Central PMCID: PMC4349583.

34. Miles R, Tóth K, Gulyás AI, Hájos N, Freund TF. Differences between Somatic and Dendritic Inhibition in the Hippocampus. Neuron. 1996;16(4):815–23. doi:10.1016/s0896-6273(00)80101-4 PubMed PMID: 8607999.

35. Katsumaru H, Kosaka T, Heizmann CW, Hama K. Immunocytochemical study of GABAergic neurons containing the calcium-binding protein parvalbumin in the rat hippocampus. Exp Brain Res. 1988;72(2):347–62. doi:10.1007/bf00250256 PubMed PMID: 3066634.

36. Ferraguti F, Cobden P, Pollard M, Cope D, Shigemoto R, Watanabe M, Somogyi P. Immunolocalization of metabotropic glutamate receptor 1α (mGluR1α) in distinct classes of interneuron in the CA1 region of the rat hippocampus. Hippocampus. 2004;14(2):193–215. doi:10.1002/hipo.10163 PubMed PMID: 15098725.

37. Blasco-Ibáñez JM, Freund TF. Synaptic Input of Horizontal Interneurons in Stratum Oriens of the Hippocampal CA1 Subfield: Structural Basis of Feed-back Activation. Eur J Neurosci. 1995;7(10):2170–80. doi:10.1111/j.1460-9568.1995.tb00638.x PubMed PMID: 8542073.

38. Frotscher M, Zimmer J. Commissural fibers terminate on non-pyramidal neurons in the guinea pig hippocampus — a combined Golgi/EM degeneration study. Brain Res. 1983;265(2):289–93. doi:10.1016/0006-8993(83)90344-x PubMed PMID: 6850332.

39. Knowles W, Schwartzkroin P. Local circuit synaptic interactions in hippocampal brain slices. J Neurosci. 1981;1(3):318–22. doi:10.1523/jneurosci.01-03-00318.1981

40. Zemankovics R, Veres JM, Oren I, Hájos N. Feedforward Inhibition Underlies the Propagation of Cholinergically Induced Gamma Oscillations from Hippocampal CA3 to CA1. J Neurosci. 2013;33(30):12337–51. doi:10.1523/jneurosci.3680-12.2013 PubMed PMID: 23884940; PubMed Central PMCID: PMC3721843.

41. Booker SA, Vida I. Morphological diversity and connectivity of hippocampal interneurons. Cell Tissue Res. 2018;373(3):619–41. doi:10.1007/s00441-018-2882-2 PubMed PMID: 30084021; PubMed Central PMCID: PMC6132631.

42. Fernández B, Jurado S, Lerma J. Understanding OLM Interneurons: Characterization, Circuitry, and Significance in Memory and Navigation. Neuroscience. 2024. doi:10.1016/j.neuroscience.2024.07.046 PubMed PMID: 39097181.

43. Gulyás AI, Mlles R, Hájos N, Freund TF. Precision and Variability in Postsynaptic Target Selection of Inhibitory Cells in the Hippocampal CA3 Region. Eur J Neurosci. 1993;5(12):1729–51. doi:10.1111/j.1460-9568.1993.tb00240.x PubMed PMID: 8124523.

44. Sik A, Penttonen M, Ylinen A, Buzsaki G. Hippocampal CA1 interneurons: an in vivo intracellular labeling study. J Neurosci. 1995;15(10):6651–65. doi:10.1523/jneurosci.15-10-06651.1995

45. Halasy K, Buhl EH, Lörinczi Z, Tamás G, Somogyi P. Synaptic target selectivity and input of GABAergic basket and bistratified interneurons in the CA1 area of the rat hippocampus. Hippocampus. 1996;6(3):306–29. doi:10.1002/(sici)1098-1063(1996)6:3<306::aid-hipo8>3.0.co;2-k PubMed PMID: 8841829.

46. Yuan M, Meyer T, Benkowitz C, Savanthrapadian S, Ansel-Bollepalli L, Foggetti A, Wulff P, Alcami P, Elgueta C, Bartos M. Somatostatin-positive interneurons in the dentate gyrus of mice provide local- and long-range septal synaptic inhibition. eLife. 2017;6:e21105. doi:10.7554/elife.21105 PubMed PMID: 28368242; PubMed Central PMCID: PMC5395294.

47. Han Z, Buhl EH, Lörinczi Z, Somogyi P. A High Degree of Spatial Selectivity in the Axonal and Dendritic Domains of Physiologically Identified Local-circuit Neurons in the Dentate Gyms of the Rat Hippocampus. Eur J Neurosci. 1993;5(5):395–410. doi:10.1111/j.1460-9568.1993.tb00507.x PubMed PMID: 8261117.

48. Halasy K, Somogyi P. Subdivisions in the Multiple GABAergic Innervation of Granule Cells in the Dentate Gyrus of the Rat Hippocampus. Eur J Neurosci. 1993;5(5):411–29. doi:10.1111/j.1460-9568.1993.tb00508.x PubMed PMID: 8261118.

49. Houser CR. Interneurons of the dentate gyrus: an overview of cell types, terminal fields and neurochemical identity. Prog Brain Res. 2007;163:217–811. doi:10.1016/s0079-6123(07)63013-1 PubMed PMID: 17765721.

50. Freund TF, Katona I. Perisomatic Inhibition. Neuron. 2007;56(1):33–42. doi:10.1016/j.neuron.2007.09.012 PubMed PMID: 17920013.

51. Cobb SR, Buhl EH, Halasy K, Paulsen O, Somogyi P. Synchronization of neuronal activity in hippocampus by individual GABAergic interneurons. Nature. 1995;378(6552):75–8. doi:10.1038/378075a0 PubMed PMID: 7477292.

52. Raudales R, Kim G, Kelly SM, Hatfield J, Guan W, Zhao S, Paul A, Qian Y, Li B, Huang ZJ. Specific and comprehensive genetic targeting reveals brain-wide distribution and synaptic input patterns of GABAergic axo-axonic interneurons. eLife. 2024;13:RP93481. doi:10.7554/elife.93481 PubMed PMID: 39012795; PubMed Central PMCID: PMC11251723.

53. Viney TJ, Lasztoczi B, Katona L, Crump MG, Tukker JJ, Klausberger T, Somogyi P. Network state-dependent inhibition of identified hippocampal CA3 axo-axonic cells in vivo. Nat Neurosci. 2013;16(12):1802–11. doi:10.1038/nn.3550 PubMed PMID: 24141313; PubMed Central PMCID: PMC4471148.

54. Soriano E, Nitsch R, Frotscher M. Axo-axonic chandelier cells in the rat fascia dentata: Golgi-electron microscopy and immunocytochemical studies. J Comp Neurol. 1990;293(1):1–25. doi:10.1002/cne.902930102 PubMed PMID: 1690225.

55. Sik A, Tamamaki N, Freund TF. Complete Axon Arborization of a Single CA3 Pyramidal Cell in the Rat Hippocampus, and its Relationship With Postsynaptic Parvalbumin-containing Interneurons. Eur J Neurosci. 1993;5(12):1719–28. doi:10.1111/j.1460-9568.1993.tb00239.x PubMed PMID: 8124522.

56. Buhl EH, Tamás G, Szilágyi T, Stricker C, Paulsen O, Somogyi P. Effect, number and location of synapses made by single pyramidal cells onto aspiny interneurones of cat visual cortex. J Physiol. 1997;500(3):689–713. doi:10.1113/jphysiol.1997.sp022053 PubMed PMID: 9161986; PubMed Central PMCID: PMC1159419.

57. McDonald AJ, Mascagni F, Mania I, Rainnie DG. Evidence for a perisomatic innervation of parvalbumin-containing interneurons by individual pyramidal cells in the basolateral amygdala. Brain Res. 2005;1035(1):32–40. doi:10.1016/j.brainres.2004.11.052 PubMed PMID: 15713274.

58. Andrási T, Veres JM, Rovira-Esteban L, Kozma R, Vikór A, Gregori E, Hájos N. Differential excitatory control of 2 parallel basket cell networks in amygdala microcircuits. PLoS Biol. 2017;15(5):e2001421. doi:10.1371/journal.pbio.2001421 PubMed PMID: 28542195; PubMed Central PMCID: PMC5443504.

59. Blasco-Ibanez JM, Martinez-Guijarro FJ, Freund TF. Recurrent mossy fibers preferentially innervate parvalbumin-immunoreactive interneurons in the granule cell layer of the rat dentate gyrus. NeuroReport. 2000;11(14):3219–25. doi:10.1097/00001756-200009280-00034 PubMed PMID: 11043552.

60. Sun Y, Grieco SF, Holmes TC, Xu X. Local and Long-Range Circuit Connections to Hilar Mossy Cells in the Dentate Gyrus. eNeuro. 2017;4(2):ENEURO.0097-17.2017. doi:10.1523/eneuro.0097-17.2017 PubMed PMID: 28451637; PubMed Central PMCID: PMC5396130.

61. Scharfman HE. The CA3 “backprojection” to the dentate gyrus. Prog Brain Res. 2007;163:627–37. doi:10.1016/s0079-6123(07)63034-9 PubMed PMID: 17765742; PubMed Central PMCID: PMC1986638.

62. Scharfman HE. Evidence from simultaneous intracellular recordings in rat hippocampal slices that area CA3 pyramidal cells innervate dentate hilar mossy cells. J Neurophysiol. 1994;72(5):2167–80. doi:10.1152/jn.1994.72.5.2167 PubMed PMID: 7884451.

63. Strowbridge BW, Buckmaster PS, Schwartzkroin PA. Potentiation of spontaneous synaptic activity in rat mossy cells. Neurosci Lett. 1992;142(2):205–10. doi:10.1016/0304-3940(92)90374-g PubMed PMID: 1454217.

64. Scharfman HE, Myers CE. Hilar mossy cells of the dentate gyrus: a historical perspective. Front Neural Circuits. 2013;6:106. doi:10.3389/fncir.2012.00106 PubMed PMID: 23420672; PubMed Central PMCID: PMC3572871.

65. Galloni AR, Samadzelkava A, Hiremath K, Oumnov R, Milstein AD. Recurrent Excitatory Feedback From Mossy Cells Enhances Sparsity and Pattern Separation in the Dentate Gyrus via Indirect Feedback Inhibition. Front Comput Neurosci. 2022;16:826278. doi:10.3389/fncom.2022.826278 PubMed PMID: 35221956; PubMed Central PMCID: PMC8866186.

66. Senzai Y, Buzsáki G. Physiological Properties and Behavioral Correlates of Hippocampal Granule Cells and Mossy Cells. Neuron. 2017;93(3):691-704.e5. doi:10.1016/j.neuron.2016.12.011 PubMed PMID: 28132824; PubMed Central PMCID: PMC5293146.

67. Hashimotodani Y, Nasrallah K, Jensen KR, Chávez AE, Carrera D, Castillo PE. LTP at Hilar Mossy Cell-Dentate Granule Cell Synapses Modulates Dentate Gyrus Output by Increasing Excitation/Inhibition Balance. Neuron. 2017;95(4):928-943.e3. doi:10.1016/j.neuron.2017.07.028 PubMed PMID: 28817805; PubMed Central PMCID: PMC5609819.

68. Buckmaster PS, Wenzel HJ, Kunkel DD, Schwartzkroin PA. Axon arbors and synaptic connections of hippocampal mossy cells in the rat in vivo. J Comp Neurol. 1996;366(2):270–92. doi:10.1002/(sici)1096-9861(19960304)366:2<270::aid-cne7>3.0.co;2-2 PubMed PMID: 8698887.

69. Swaminathan A, Wichert I, Schmitz D, Maier N. Involvement of Mossy Cells in Sharp Wave-Ripple Activity In Vitro. Cell Rep. 2018;23(9):2541–9. doi:10.1016/j.celrep.2018.04.095 PubMed PMID: 29847786.

70. GoodSmith D, Chen X, Wang C, Kim SH, Song H, Burgalossi A, Christian KM, Knierim JJ. Spatial Representations of Granule Cells and Mossy Cells of the Dentate Gyrus. Neuron. 2017;93(3):677-690.e5. doi:10.1016/j.neuron.2016.12.026 PubMed PMID: 28132828; PubMed Central PMCID: PMC5300955.

71. Bui AD, Nguyen TM, Limouse C, Kim HK, Szabo GG, Felong S, Maroso M, Soltesz I. Dentate gyrus mossy cells control spontaneous convulsive seizures and spatial memory. Science. 2018;359(6377):787–90. doi:10.1126/science.aan4074 PubMed PMID: 29449490; PubMed Central PMCID: PMC6040648.

72. Blümcke I, Suter B, Behle K, Kuhn R, Schramm J, Elger CE, Wiestler OD. Loss of Hilar Mossy Cells in Ammon's Horn Sclerosis. Epilepsia. 2000;41(s6):S174–80. doi:10.1111/j.1528-1157.2000.tb01577.x PubMed PMID: 10999540.

73. Amaral DG, Scharfman HE, Lavenex P. The dentate gyrus: fundamental neuroanatomical organization (dentate gyrus for dummies). Prog Brain Res. 2007;163:3–790. doi:10.1016/s0079-6123(07)63001-5 PubMed PMID: 17765709; PubMed Central PMCID: PMC2492885.

74. Chicurel ME, Harris KM. Three-dimensional analysis of the structure and composition of CA3 branched dendritic spines and their synaptic relationships with mossy fiber boutons in the rat hippocampus. J Comp Neurol. 1992;325(2):169–82. doi:10.1002/cne.903250204 PubMed PMID: 1460112.

75. Toth K, Suares G, Lawrence JJ, Philips-Tansey E, McBain CJ. Differential Mechanisms of Transmission at Three Types of Mossy Fiber Synapse. J Neurosci. 2000;20(22):8279–89. doi:10.1523/jneurosci.20-22-08279.2000

76. Vyleta NP, Borges-Merjane C, Jonas P. Plasticity-dependent, full detonation at hippocampal mossy fiber–CA3 pyramidal neuron synapses. eLife. 2016;5:e17977. doi:10.7554/elife.17977 PubMed PMID: 27780032; PubMed Central PMCID: PMC5079747.

77. Erwin SR, Sun W, Copeland M, Lindo S, Spruston N, Cembrowski MS. A Sparse, Spatially Biased Subtype of Mature Granule Cell Dominates Recruitment in Hippocampal-Associated Behaviors. Cell Rep. 2020;31(4):107551. doi:10.1016/j.celrep.2020.107551 PubMed PMID: 32348756.

78. Williams PA, Larimer P, Gao Y, Strowbridge BW. Semilunar Granule Cells: Glutamatergic Neurons in the Rat Dentate Gyrus with Axon Collaterals in the Inner Molecular Layer. J Neurosci. 2007;27(50):13756–61. doi:10.1523/jneurosci.4053-07.2007 PubMed PMID: 18077687; PubMed Central PMCID: PMC6673630.

79. Save L, Baude A, Cossart R. Temporal Embryonic Origin Critically Determines Cellular Physiology in the Dentate Gyrus. Cereb Cortex. 2019;29(6):2639–52. doi:10.1093/cercor/bhy132 PubMed PMID: 29878074.

80. Afrasiabi M, Gupta A, Xu H, Swietek B, Santhakumar V. Differential Activity-Dependent Increase in Synaptic Inhibition and Parvalbumin Interneuron Recruitment in Dentate Granule Cells and Semilunar Granule Cells. J Neurosci. 2022;42(6):1090–103. doi:10.1523/jneurosci.1360-21.2021 PubMed PMID: 34980636; PubMed Central PMCID: PMC8824497.

81. Dovek L, Marrero K, Zagha E, Santhakumar V. Cellular and circuit features distinguish dentate gyrus semilunar granule cells and granule cells activated during contextual memory formation. 2024. doi:10.7554/elife.101428.1

82. Larimer P, Strowbridge BW. Representing information in cell assemblies: persistent activity mediated by semilunar granule cells. Nat Neurosci. 2010;13(2):213–22. doi:10.1038/nn.2458 PubMed PMID: 20037579; PubMed Central PMCID: PMC2840722.

83. Goaillard JM, Marder E. Ion Channel Degeneracy, Variability, and Covariation in Neuron and Circuit Resilience. Annu Rev Neurosci. 2021;44(1):1–23. doi:10.1146/annurev-neuro-092920-121538 PubMed PMID: 33770451.

84. Ramsey IS, Delling M, Clapham DE. AN INTRODUCTION TO TRP CHANNELS. Annu Rev Physiol. 2006;68(1):619–47. doi:10.1146/annurev.physiol.68.040204.100431 PubMed PMID: 16460286.

85. Tang Q, Guo W, Zheng L, Wu JX, Liu M, Zhou X, Zhang X, Chen L. Structure of the receptor-activated human TRPC6 and TRPC3 ion channels. Cell Res. 2018;28(7):746–55. doi:10.1038/s41422-018-0038-2 PubMed PMID: 29700422; PubMed Central PMCID: PMC6028632.

86. Clapham DE. TRP channels as cellular sensors. Nature. 2003;426(6966):517–24. doi:10.1038/nature02196 PubMed PMID: 14654832.

87. Owsianik G, D'hoedt D, Voets T, Nilius B. Reviews of Physiology, Biochemistry and Pharmacology. 2006;61–90. doi:10.1007/s10254-005-0006-0

88. Hofmann T, Obukhov AG, Schaefer M, Harteneck C, Gudermann T, Schultz G. Direct activation of human TRPC6 and TRPC3 channels by diacylglycerol. Nature. 1999;397(6716):259–63. doi:10.1038/16711 PubMed PMID: 9930701.

89. Bollimuntha S, Selvaraj S, Singh BB. Transient Receptor Potential Channels. Adv Exp Med Biol. 2010;704:573–93. doi:10.1007/978-94-007-0265-3_31 PubMed PMID: 21290317; PubMed Central PMCID: PMC3045772.

90. Zernov N, Popugaeva E. Role of Neuronal TRPC6 Channels in Synapse Development, Memory Formation and Animal Behavior. Int J Mol Sci. 2023;24(20):15415. doi:10.3390/ijms242015415 PubMed PMID: 37895105; PubMed Central PMCID: PMC10607207.

91. Russo E, Scicchitano F, Whalley BJ, Mazzitello C, Ciriaco M, Esposito S, Patanè M, Upton R, Pugliese M, Chimirri S, Mammì M, Palleria C, Sarro GD. Hypericum perforatum: Pharmacokinetic, Mechanism of Action, Tolerability, and Clinical Drug–Drug Interactions. Phytotherapy Res. 2014;28(5):643–55. doi:10.1002/ptr.5050 PubMed PMID: 23897801.

92. Leuner K, Kazanski V, Muller M, Essin K, Henke B, Gollasch M, Harteneck C, Müller WE. Hyperforin—a key constituent of St. John's wort specifically activates TRPC6 channels. FASEB J. 2007;21(14):4101–11. doi:10.1096/fj.07-8110com PubMed PMID: 17666455.

93. Beis D, Schwarting RKW, Dietrich A. Evidence for a supportive role of classical transient receptor potential 6 (TRPC6) in the exploration behavior of mice. Physiol Behav. 2011;102(2):245–50. doi:10.1016/j.physbeh.2010.11.002 PubMed PMID: 21059368.

94. Zhou J, Du W, Zhou K, Tai Y, Yao H, Jia Y, Ding Y, Wang Y. Critical role of TRPC6 channels in the formation of excitatory synapses. Nat Neurosci. 2008;11(7):741–3. doi:10.1038/nn.2127 PubMed PMID: 18516035.

95. Tai Y, Feng S, Ge R, Du W, Zhang X, He Z, Wang Y. TRPC6 channels promote dendritic growth via the CaMKIV-CREB pathway. J Cell Sci. 2008;121(14):2301–7. doi:10.1242/jcs.026906 PubMed PMID: 18559891.

96. Berna-Erro A, Jardin I, Salido GM, Rosado JA. Role of STIM2 in cell function and physiopathology. J Physiol. 2017;595(10):3111–28. doi:10.1113/jp273889 PubMed PMID: 28087881; PubMed Central PMCID: PMC5430229.

97. Bisogno T, Howell F, Williams G, Minassi A, Cascio MG, Ligresti A, Matias I, Schiano-Moriello A, Paul P, Williams EJ, Gangadharan U, Hobbs C, Marzo VD, Doherty P. Cloning of the first sn1-DAG lipases points to the spatial and temporal regulation of endocannabinoid signaling in the brain. J Cell Biol. 2003;163(3):463–8. doi:10.1083/jcb.200305129 PubMed PMID: 14610053; PubMed Central PMCID: PMC2173631.

98. Katona I, Freund TF. Endocannabinoid signaling as a synaptic circuit breaker in neurological disease. Nat Med. 2008;14(9):923–30. doi:10.1038/nm.f.1869 PubMed PMID: 18776886.

99. Luján R, Nusser Z, Roberts JDB, Shigemoto R, Somogyi P. Perisynaptic Location of Metabotropic Glutamate Receptors mGluR1 and mGluR5 on Dendrites and Dendritic Spines in the Rat Hippocampus. Eur J Neurosci. 1996;8(7):1488–500. doi:10.1111/j.1460-9568.1996.tb01611.x PubMed PMID: 8758956.

100. Luján R, Roberts JDB, Shigemoto R, Ohishi H, Somogyi P. Differential plasma membrane distribution of metabotropic glutamate receptors mGluR1α, mGluR2 and mGluR5, relative to neurotransmitter release sites. J Chem Neuroanat. 1997;13(4):219–41. doi:10.1016/s0891-0618(97)00051-3 PubMed PMID: 9412905.

101. Fukaya M, Uchigashima M, Nomura S, Hasegawa Y, Kikuchi H, Watanabe M. Predominant expression of phospholipase Cβ1 in telencephalic principal neurons and cerebellar interneurons, and its close association with related signaling molecules in somatodendritic neuronal elements. Eur J Neurosci. 2008;28(9):1744–59. doi:10.1111/j.1460-9568.2008.06495.x PubMed PMID: 18973591.

102. Katona I, Urbán GM, Wallace M, Ledent C, Jung KM, Piomelli D, Mackie K, Freund TF. Molecular Composition of the Endocannabinoid System at Glutamatergic Synapses. J Neurosci. 2006;26(21):5628–37. doi:10.1523/jneurosci.0309-06.2006 PubMed PMID: 16723519; PubMed Central PMCID: PMC1698282.

103. Yoshida T, Fukaya M, Uchigashima M, Miura E, Kamiya H, Kano M, Watanabe M. Localization of Diacylglycerol Lipase-α around Postsynaptic Spine Suggests Close Proximity between Production Site of an Endocannabinoid, 2-Arachidonoyl-glycerol, and Presynaptic Cannabinoid CB1 Receptor. J Neurosci. 2006;26(18):4740–51. doi:10.1523/jneurosci.0054-06.2006 PubMed PMID: 16672646; PubMed Central PMCID: PMC6674155.

104. Bardell TK, Barker EL. Activation of TRPC6 channels promotes endocannabinoid biosynthesis in neuronal CAD cells. Neurochem Int. 2010;57(1):76–83. doi:10.1016/j.neuint.2010.05.002 PubMed PMID: 20466028; PubMed Central PMCID: PMC2897062.

105. Rovira-Esteban L, Hájos N, Nagy GA, Crespo C, Nacher J, Varea E, Blasco-Ibáñez JM. Semilunar Granule Cells Are the Primary Source of the Perisomatic Excitatory Innervation onto Parvalbumin-Expressing Interneurons in the Dentate Gyrus. eNeuro. 2020;7(4):ENEURO.0323-19.2020. doi:10.1523/eneuro.0323-19.2020 PubMed PMID: 32571963; PubMed Central PMCID: PMC7340841.

106. Spruston N, Johnston D. Perforated patch-clamp analysis of the passive membrane properties of three classes of hippocampal neurons. J Neurophysiol. 1992;67(3):508–29. doi:10.1152/jn.1992.67.3.508 PubMed PMID: 1578242.

107. Staley KJ, Otis TS, Mody I. Membrane properties of dentate gyrus granule cells: comparison of sharp microelectrode and whole-cell recordings. J Neurophysiol. 1992;67(5):1346–58. doi:10.1152/jn.1992.67.5.1346 PubMed PMID: 1597717.

108. Penttonen M, Kamondi A, Sik A, Acsády L, Buzsáki G. Feed-forward and feed-back activation of the dentate gyrus in vivo during dentate spikes and sharp wave bursts. Hippocampus. 1997;7(4):437–50. doi:10.1002/(sici)1098-1063(1997)7:4<437::aid-hipo9>3.0.co;2-f PubMed PMID: 9287083.

109. SHOLL DA, UTTLEY AM. Pattern Discrimination and the Visual Cortex. Nature. 1953;171(4348):387–8. doi:10.1038/171387a0 PubMed PMID: 13036904.

110. Nagy GA, Botond G, Borhegyi Z, Plummer NW, Freund TF, Hájos N. DAG-sensitive and Ca2+ permeable TRPC6 channels are expressed in dentate granule cells and interneurons in the hippocampal formation. Hippocampus. 2013;23(3):221–32. doi:10.1002/hipo.22081 PubMed PMID: 23193081; PubMed Central PMCID: PMC3586768.

111. Tanaka J, Nakagawa S, Kushiya E, Yamasaki M, Fukaya M, Iwanaga T, Simon MI, Sakimura K, Kano M, Watanabe M. Gq protein α subunits Gαq and Gα11 are localized at postsynaptic extra-junctional membrane of cerebellar Purkinje cells and hippocampal pyramidal cells. Eur J Neurosci. 2000;12(3):781–92. doi:10.1046/j.1460-9568.2000.00959.x PubMed PMID: 10762307.

112. Timm F. Zur Histochemie des Zinks. Dtsch Z für die gesamte Gerichtl Med. 1958;47(3):428–31. doi:10.1007/bf00664118 PubMed PMID: 13597636.

113. Laurberg S, Zimmer J. Lesion-induced sprouting of hippocampal mossy fiber collaterals to the fascia dentata in developing and adult rats. J Comp Neurol. 1981;200(3):433–59. doi:10.1002/cne.902000310 PubMed PMID: 7276246.

114. Frotscher M, Jonas P, Sloviter RS. Synapses formed by normal and abnormal hippocampal mossy fibers. Cell Tissue Res. 2006;326(2):361–7. doi:10.1007/s00441-006-0269-2 PubMed PMID: 16819624.

115. Gulyás AI, Hájos N, Freund TF. Interneurons Containing Calretinin Are Specialized to Control Other Interneurons in the Rat Hippocampus. J Neurosci. 1996;16(10):3397–411. doi:10.1523/jneurosci.16-10-03397.1996

116. Gulyás AI, Buzsáki G, Freund TF, Hirase H. Populations of hippocampal inhibitory neurons express different levels of cytochrome c. Eur J Neurosci. 2006;23(10):2581–94. doi:10.1111/j.1460-9568.2006.04814.x PubMed PMID: 16817861.

117. Nahirney PC, Tremblay ME. Brain Ultrastructure: Putting the Pieces Together. Front Cell Dev Biol. 2021;9:629503. doi:10.3389/fcell.2021.629503 PubMed PMID: 33681208; PubMed Central PMCID: PMC7930431.

118. Dietrich A, Schnitzler MM y, Gollasch M, Gross V, Storch U, Dubrovska G, Obst M, Yildirim E, Salanova B, Kalwa H, Essin K, Pinkenburg O, Luft FC, Gudermann T, Birnbaumer L. Increased Vascular Smooth Muscle Contractility in TRPC6 − / − Mice. Mol Cell Biol. 2005;25(16):6980–9. doi:10.1128/mcb.25.16.6980-6989.2005 PubMed PMID: 16055711; PubMed Central PMCID: PMC1190236.

119. Baude A, Nusser Z, Roberts JDB, Mulvihill E, Mcllhinney RAJ, Somogyi P. The metabotropic glutamate receptor (mGluRlα) is concentrated at perisynaptic membrane of neuronal subpopulations as detected by immunogold reaction. Neuron. 1993;11(4):771–87. doi:10.1016/0896-6273(93)90086-7 PubMed PMID: 8104433.

120. Takács VT, Klausberger T, Somogyi P, Freund TF, Gulyás AI. Extrinsic and local glutamatergic inputs of the rat hippocampal CA1 area differentially innervate pyramidal cells and interneurons. Hippocampus. 2012;22(6):1379–91. doi:10.1002/hipo.20974 PubMed PMID: 21956752; PubMed Central PMCID: PMC4473063.

121. Ribak CE, Peterson GM. Intragranular mossy fibers in rats and gerbils from synapses with the somata and proximal dendrites of basket cells in the dentate gyrus. Hippocampus. 1991;1(4):355–64. doi:10.1002/hipo.450010403 PubMed PMID: 1669315.

122. Seress L, Ábrahám H, Paleszter M, Gallyas F. Granule cells are the main source of excitatory input to a subpopulation of GABAergic hippocampal neurons as revealed by electron microscopic double staining for zinc histochemistry and parvalbumin immunocytochemistry. Exp Brain Res. 2001;136(4):456–62. doi:10.1007/s002210000601 PubMed PMID: 11291726.

123. Gupta A, Elgammal FS, Proddutur A, Shah S, Santhakumar V. Decrease in Tonic Inhibition Contributes to Increase in Dentate Semilunar Granule Cell Excitability after Brain Injury. J Neurosci. 2012;32(7):2523–37. doi:10.1523/jneurosci.4141-11.2012 PubMed PMID: 22396425; PubMed Central PMCID: PMC6621807.

124. Espinoza C, Guzman SJ, Zhang X, Jonas P. Parvalbumin+ interneurons obey unique connectivity rules and establish a powerful lateral-inhibition microcircuit in dentate gyrus. Nat Commun. 2018;9(1):4605. doi:10.1038/s41467-018-06899-3 PubMed PMID: 30389916; PubMed Central PMCID: PMC6214995.

125. GoodSmith D, Lee H, Neunuebel JP, Song H, Knierim JJ. Dentate Gyrus Mossy Cells Share a Role in Pattern Separation with Dentate Granule Cells and Proximal CA3 Pyramidal Cells. J Neurosci. 2019;39(48):9570–84. doi:10.1523/jneurosci.0940-19.2019 PubMed PMID: 31641051; PubMed Central PMCID: PMC6880467.

126. Nakazawa K. Dentate Mossy Cell and Pattern Separation. Neuron. 2017;93(3):465–7. doi:10.1016/j.neuron.2017.01.021 PubMed PMID: 28182899.

127. Aires V, Hichami A, Boulay G, Khan NA. Activation of TRPC6 calcium channels by diacylglycerol (DAG)-containing arachidonic acid: A comparative study with DAG-containing docosahexaenoic acid. Biochimie. 2007;89(8):926–37. doi:10.1016/j.biochi.2006.10.016 PubMed PMID: 17532549.

128. Nakamura M, Sato K, Fukaya M, Araishi K, Aiba A, Kano M, Watanabe M. Signaling complex formation of phospholipase Cβ4 with metabotropic glutamate receptor type 1α and 1,4,5-trisphosphate receptor at the perisynapse and endoplasmic reticulum in the mouse brain. Eur J Neurosci. 2004;20(11):2929–44. doi:10.1111/j.1460-9568.2004.03768.x PubMed PMID: 15579147.

129. Shigemoto R, Kinoshita A, Wada E, Nomura S, Ohishi H, Takada M, Flor PJ, Neki A, Abe T, Nakanishi S, Mizuno N. Differential Presynaptic Localization of Metabotropic Glutamate Receptor Subtypes in the Rat Hippocampus. J Neurosci. 1997;17(19):7503–22. doi:10.1523/jneurosci.17-19-07503.1997

130. Uchigashima M, Yamazaki M, Yamasaki M, Tanimura A, Sakimura K, Kano M, Watanabe M. Molecular and Morphological Configuration for 2-Arachidonoylglycerol-Mediated Retrograde Signaling at Mossy Cell–Granule Cell Synapses in the Dentate Gyrus. J Neurosci. 2011;31(21):7700–14. doi:10.1523/jneurosci.5665-10.2011 PubMed PMID: 21613483; PubMed Central PMCID: PMC6633146.

131. Drake CT, Milner TA, Patterson SL. Ultrastructural Localization of Full-Length trkB Immunoreactivity in Rat Hippocampus Suggests Multiple Roles in Modulating Activity-Dependent Synaptic Plasticity. J Neurosci. 1999;19(18):8009–26. doi:10.1523/jneurosci.19-18-08009.1999 PubMed PMID: 10479701.

132. Cahalan MD. STIMulating store-operated Ca2+ entry. Nat Cell Biol. 2009;11(6):669–77. doi:10.1038/ncb0609-669 PubMed PMID: 19488056; PubMed Central PMCID: PMC2721799.

133. Pani B, Bollimuntha S, Singh BB. The TR (i)P to Ca2+ signaling just got STIMy: an update on STIM1 activated TRPC channels. Front Biosci. 2012;17(1):805. doi:10.2741/3958 PubMed PMID: 22201775; PubMed Central PMCID: PMC3293191.

134. Shimizu H, Fukaya M, Yamasaki M, Watanabe M, Manabe T, Kamiya H. Use-dependent amplification of presynaptic Ca2+ signaling by axonal ryanodine receptors at the hippocampal mossy fiber synapse. Proc Natl Acad Sci. 2008;105(33):11998–2003. doi:10.1073/pnas.0802175105 PubMed PMID: 18687898; PubMed Central PMCID: PMC2575294.

135. Hooft JA van, Giuffrida R, Blatow M, Monyer H. Differential Expression of Group I Metabotropic Glutamate Receptors in Functionally Distinct Hippocampal Interneurons. J Neurosci. 2000;20(10):3544–51. doi:10.1523/jneurosci.20-10-03544.2000

136. Topolnik L, Azzi M, Morin F, Kougioumoutzakis A, Lacaille J. mGluR1/5 subtype-specific calcium signalling and induction of long-term potentiation in rat hippocampal oriens/alveus interneurones. J Physiol. 2006;575(1):115–31. doi:10.1113/jphysiol.2006.112896 PubMed PMID: 16740609; PubMed Central PMCID: PMC1819425.

137. Pouille F, Scanziani M. Routing of spike series by dynamic circuits in the hippocampus. Nature. 2004;429(6993):717–23. doi:10.1038/nature02615 PubMed PMID: 15170216.

## 9. BIBLIOGRAPHY OF THE CANDIDATE'S PUBLICATIONS

Related to the thesis:

**Nagy, G. A.,** Botond, G., Borhegyi, Z., Plummer, N. W., Freund, T. F., & Hájos, N. (2013). DAG-sensitive and Ca2+ permeable TRPC6 channels are expressed in dentate granule cells and interneurons in the hippocampal formation. *Hippocampus*, *23*(3), 221-232. https://doi.org/10.1002/hipo.22081

Rovira-Esteban, L., Hájos, N., **Nagy, G. A**., Crespo, C., Nacher, J., Varea, E., & Blasco-Ibáñez, J. M. (2020). Semilunar granule cells are the primary source of the perisomatic excitatory innervation onto parvalbumin-expressing interneurons in the dentate gyrus. *Eneuro*, *7*(4). https://doi.org/10.1523/ENEURO.0323-19.2020

Unrelated to the thesis:

Robinson, H. L., Todorova, R., **Nagy, G. A.**, Gruzdeva, A., Paudel, P., Oliva, A., & Fernandez-Ruiz, A. (2026). Large sharp-wave ripples promote hippocampo-cortical memory reactivation and consolidation during sleep. *Neuron*, *114*(2), 226-236. 10.1016/j.neuron.2025.10.003

Fernández-Ruiz, A., Oliva, A., Soula, M., Rocha-Almeida, F., **Nagy, G. A**., Martin-Vazquez, G., & Buzsáki, G. (2021). Gamma rhythm communication between entorhinal cortex and dentate gyrus neuronal assemblies. *Science*, *372*(6537). https://doi.org/10.1126/science.abf3119

Fernández-Ruiz, A., Oliva, A., **Nagy, G. A**., Maurer, A. P., Berényi, A., & Buzsáki, G. (2017). Entorhinal- CA3 dual-input control of spike timing in the hippocampus by theta-gamma coupling. *Neuron*, *93*(5), 1213-1226. https://doi.org/10.1016/j.neuron.2017.02.017

Veres, J. M., **Nagy, G. A**., & Hajos, N. (2017). Perisomatic GABAergic synapses of basket cells effectively control principal neuron activity in amygdala networks. *Elife*, *6*, e20721. https://doi.org/10.7554/eLife.20721.001

Vereczki, V. K., Veres, J. M., Müller, K., **Nagy, G. A**., Rácz, B., Barsy, B., & Hájos, N. (2016). Synaptic organization of perisomatic GABAergic inputs onto the principal cells of the mouse basolateral amygdala. *Frontiers in neuroanatomy*, *10*, 20. https://doi.org/10.3389/fnana.2016.00020

Veres, J. M., **Nagy, G. A**., Vereczki, V. K., Andrási, T., & Hájos, N. (2014). Strategically positioned inhibitory synapses of axo-axonic cells potently control principal neuron spiking in the basolateral amygdala. *Journal of Neuroscience*, *34*(49), 16194-16206. https://doi.org/10.1523/JNEUROSCI.2232-14.2014

Holderith, N., Németh, B., Papp, O. I., Veres, J. M., **Nagy, G. A**., & Hájos, N. (2011). Cannabinoids attenuate hippocampal gamma oscillations by suppressing excitatory synaptic input onto CA3 pyramidal neurons and fast spiking basket cells. *The Journal of physiology*, *589*(20), 4921-4934. https://doi.org/10.1113/jphysiol.2011.216259

## 10. ACKNOWLEDGEMENTS

Mindenekelőtt köszönöm a családomnak, Fenyvesi Enikőnek és Nagy Bencének, hogy ilyen kitartóan támogattak és támogatnak a céljaim elérésében. Nélkülük ez a dolgozat nem készült volna el.

Köszönöm egykori tanáromnak, Horváth Kálmánnak, hogy elindított a pályán és Lengyel Katalinnak, akitől életem első idegtudományi vizsgálómódszereit tanultam.

Furthermore, I would like to thank Cecília Pardo-Bellver for the invaluable help and for being a true inspiration during my PhD research, and I'd like to thank both Cecília Pardo-Bellver, Sergio Martinez-Bellver and Müller Kinga for their professional support and invaluable friendship.

I would like to thank Mihály Vöröslakos, Azahara Oliva, Antonio Fernández-Ruiz and Gábor Kozák for their continued help, guidance and friendship throughout my scientific journey.

I would also like to thank Viktor Varga, Márta Jelitai, Tiago Chaves and Rita Nyilas for their support during the final phase of my PhD.